LA-UR--90-3495

DE91 001967

TITLE: MONTE CARLO METHODS AND APPLICATIONS IN NUCLEAR PHYSICS

AUTHOR(S):   J. Carlson, T-5

SUBMITTED TO: PROCEEDINGS OF THE INTERNATIONAL SUMMER SCHOOL ON THE
STRUCTURE OF HADRONS AND HADRONIC MATTER, DRONTEN
THE NETHERLANDS, AUGUST 4-17, 1990, GIVEN AS AN
INVITED SET OF TALKS

Received by OSTI

NOV 0 5 1990

Los Alamos

Los Alamos National Laboratory
Los Alamos, New Mexico 87545

MONTE CARLO METHODS and APPLICATIONS IN NUCLEAR PHYSICS

J. Carlson
T5 Mail Stop B283
Los Alamos National Lab
Los Alamos, NM 87545

Abstract

Monte Carlo methods for studying few- and many-body quantum systems are introduced, with special emphasis given to their applications in nuclear physics. Variational and Green's function Monte Carlo methods are presented in some detail. The status of calculations of light nuclei is reviewed, including discussions of the three-nucleon-interaction, charge and magnetic form factors, the coulomb sum rule, and studies of low-energy radiative transitions.

1. Introduction

In these lectures I will introduce Monte Carlo methods as applied to few- and many-body quantum systems, and in particular to few-body problems in nuclear physics. While I will not be able to go into some of the technical details, I hope to provide you with a basic understanding of the principles involved. I also hope to convince you that there are many intriguing questions that can be addressed by studying light nuclei, and that Monte Carlo methods provide a useful way of attacking these few-body problems.

I will discuss Variational[1-4] (VMC) and Green's function Monte Carlo[5-7] (GFMC). VMC and GFMC are fairly general; they are often used in condensed matter[8-11] and atomic physics[12,13] in addition to their applications in nuclear physics. These methods are also closely related to the finite temperature methods used in both condensed matter and lattice QCD. Nuclear physics applications include hypernuclei and various constituent quark models in addition to light nuclei. Attempts are also being made to apply generalizations of these methods to heavier nuclei, but I will restrict myself to few-body problems in these lectures.

I will also cover the structure of the ground states of light nuclei, including two-body correlations, the importance of the tensor force, and the effect of three-nucleon interactions. I will present calculations of the Coulomb sum, one of the best experimental[14-16] indications of strong correlations within the nucleus. In addition, I will touch upon models of the currents, including two body charge and current operators,

and their importance in describing electromagnetic form factors. Finally, I will look at Monte Carlo methods for calculating low-energy scattering; and in particular at recent calculations of neutron radiative capture on ^{3}He.

First, however, I will present the basic Monte Carlo algorithms. The most important principles will be described along with the simplest practical algorithms. These tools should allow you to explore at least simple systems on your own. One should always keep in mind, though, that for more complicated problems, better Monte Carlo methods (improved sampling techniques, etc.) can be vital, making the difference between a robust solution with good statistical accuracy and a result with statistical errors so large as to render the calculation virtually meaningless. I hope that the references will be sufficient in number and detail to allow anyone interested to easily go beyond the relatively crude algorithms given here.

2. Nuclear Hamiltonian

Before studying the Monte Carlo algorithms, I would like to spend a little time discussing the nuclear Hamiltonian and the difficulties involved in determining its eigenstates. We will employ the traditional description of the nucleus as a system of non-relativistic nucleons interacting through strong spin- and isospin-dependent nuclear interactions. The solutions of the Schroedinger equation

$$H|\Psi\rangle = \left[\sum_i -\frac{\hbar^2}{2m}\nabla_i^2 + \sum_{i<j} V_{ij} + \sum_{i<j<k} V_{ijk} + ...\right]\Psi = E|\Psi\rangle \tag{1}$$

can then be used, along with an appropriate current operator, to determine many properties of the nucleus. The potential is determined by fitting two- (and possibly three-) body experimental data. It includes the one-pion-exchange term at long distances, and in some cases is modeled as a set of one-boson exchanges at shorter distances. Clearly this model leaves out some interesting physics; internal degrees of freedom (such as the delta resonance) have been suppressed and the effects of meson exchange have been absorbed into the potential. Each of these simplifications produces important effects even in ground-state properties, as we shall see. Nevertheless, even this simple non-relativistic treatment contains a great deal of physics.

The two-body interaction can be written as a sum of spin-isospin dependent operator O_{ij}^k multiplied by functions of the pair separation r_{ij}:

$$V_{ij} = \sum_{i<j} V^k(r_{ij})O_{ij}^k. \tag{2}$$

where the operators O_{ij}^k are

$$O_{ij}^k = \{1, \sigma_i \cdot \sigma_j, S_{ij}, L \cdot S_{ij}, L \cdot S_{ij}^2, L_{ij}^2, L_{ij}^2\sigma_i \cdot \sigma_j\} \bigotimes \{1, \tau_i \cdot \tau_j\} \tag{3}$$

where the symbol $\otimes$ indicates all products of one term in the first bracket and one term in the second. In this expression, σ_i and σ_j are Pauli matrices representing the

spins of the nucleons, and τ_i and τ_j are similar matrices for the isospins. The tensor operator S_{ij} is $3\sigma_i \cdot \hat{r}_{ij}\sigma_j \cdot \hat{r}_{ij} - \sigma_i \cdot \sigma_j$ and $L \cdot S_{ij}$ is the spin-orbit interaction, where L represents the relative angular momentum of the pair, and S the total spin. The operators $L \cdot S_{ij}^2$ and L_{ij}^2 determine the spin-orbit squared and angular momentum squared dependence of the interaction, respectively.

All modern interactions (Argonne,[17] Bonn,[18] Nijmegen[19] ...) may be written in a similar manner. Terms up to first order in the momentum $(L \cdot S_{ij})$ are uniquely indicated by the data, but the choice of the more non-local operators varies in different interaction models. We will concentrate primarily upon the Argonne V14 interaction which employs the particular choice given above. It has been constructed to minimize the importance of the non-local terms in the interaction, and includes a one-pion interaction at long distances, an intermediate range attraction with the range of a two-pion-exchange, and a short-range phenomenological repulsion.

Some terms in the Argonne V14 interaction are shown in figure 1, for simplicity I only present the central (momentum-independent) and tensor terms in the interaction. Two primary features that are common to all NN interaction models should be stressed. The most striking feature is the strong repulsive core at short distances. This presents some difficulties to mean-field or perturbative calculations, but it is possible to treat the strong correlations induced by these interactions with Monte Carlo. In fact, I will show results from condensed matter physics for systems of fifty to several hundred very strongly-interacting particles. The repulsive core in these systems is even stronger, in relative terms, than that in the NN interaction.
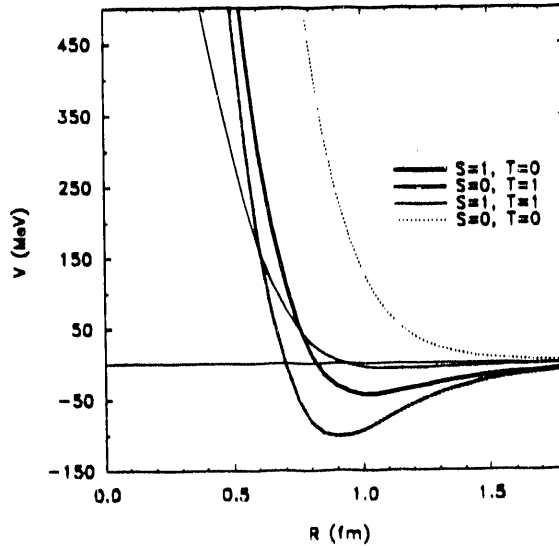

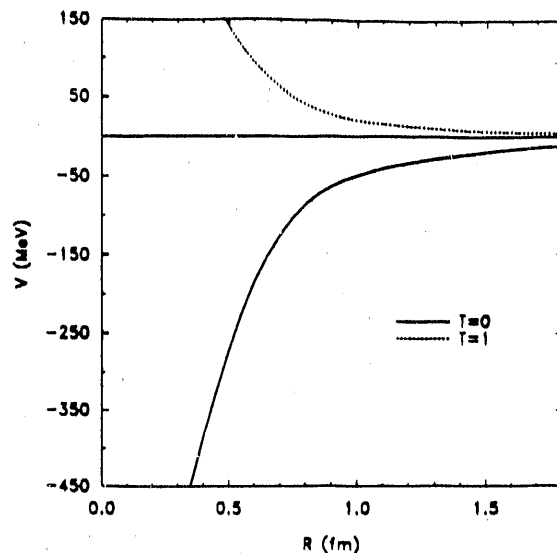Figure 1a) Central terms in the Argonne V14 interaction.

Figure 1b) Tensor terms in the Argonne V14 interaction.

The second feature, also crucial to nuclear physics, is the strong spin- and isospin-dependence of the interaction. The potential can be quite different for different combinations of total spin and isospin (note that the S,T = 0,0 and 1,1 central terms occur in negative parity states, and consequently always appear in combination with L_{ij}^2 terms). Results are also very sensitive to the tensor force, in fact we find that the tensor force provides about 2/3 of the total potential energy in light nuclei. Consequently, any wave function which ignores the strong tensor correlations will not reproduce any of the bound states. The strong state-dependence of the interaction is also what limits our calculations to light nuclei, at least for the present. To understand why, we will need to look at the structure of the wave function.

Before proceeding to the wave function, though, I should mention the three-nucleon interaction (TNI). The TNI will be discussed in more detail in a later section, at this point I would simply point out that the presence of a three nucleon interaction is essentially required by the fact that we are suppressing the internal structure of the nucleons. The importance of the three-nucleon interaction (TNI) can be taken as a measure of the importance of ignoring the internal degrees of freedom in the nucleon, the quarks. At long distances the form of the TNI is assumed to arise from pion exchanges and excitations to virtual deltas, its precise strength is fit to the three-body binding energy.[2] We will find that the TNI is much less important than the two-nucleon interaction, typically $\langle V_{ijk}\rangle/\langle V_{ij}\rangle \leq 5\%$. However, it does provide a significant fraction of the binding energy in light nuclei, as the binding energy results from a sensitive cancellation of large kinetic and potential energy terms.

4

3. Variational Wave Functions

Given the Hamiltonian of Eqs. 1 - 3, any wave function can be decomposed into a sum over spin-isospin states times functions of the coordinates of all particles:

$$|\Psi\rangle = \sum_l \psi_l(\mathbf{R})\chi_l. \tag{4}$$

The sum over states l runs from 1 to $2^A A!/N!Z!$ for a system of N neutrons and Z protons (A=N+Z). The factor 2^A comes from the spins (each of A spins up or down) and a factor of $A!/N!Z!$ from the isospin. The isospin factor is smaller because of charge conservation, the total number of protons or neutrons remains constant. Note that we are not exploiting good overall isospin, which could reduce the number of components further at the cost of a more complicated basis. Calculations employ a basis of definite third components of spin and isospin for each particle. This is discussed in more detail in the Appendix.

Solving the Schroedinger equation now entails solving many coupled differential equations for the complex amplitudes $\psi_l(\mathbf{R})$. For A=3, Faddeev methods[20-22] can be used to solve for these amplitudes explicitly, although they of course employ a different basis of states. As the number of nucleons increases, however, it becomes less and less feasible to solve directly for the amplitudes ψ_l. One possibility for going to larger systems is to develop approximate variational solutions for the wave function, this is the alternative we will discuss first. Note that the three-body nuclei provide a very important test for any variational calculation since they can be calculated 'exactly' with Faddeev methods.

Any variational calculations proceeds by first making an ansatz for the form of the wave function and then minimizing the expectation value of the Hamiltonian

$$\langle H \rangle = \frac{\langle \Psi_T\{\alpha\}| H |\Psi_T\{\alpha\}\rangle}{\langle \Psi_T\{\alpha\}\Psi_T\{\alpha\}\rangle} \tag{5}$$

with respect to changes in the variational parameters $\{\alpha\}$ embedded in the form of variational (trial) wave function $\Psi_T\{\alpha\}$. The important physics required in this case includes (1) an accurate form for the wave function as two nucleons are brought close together, (2) a reasonable treatment of the spin-isospin correlations induced by the interaction, and (3) the correct asymptotic wave function as one nucleon is pulled away from the remaining nucleons.

A generalized Jastrow form for the wave function can be used which incorporates all of this physics:

$$|\Psi_T\rangle = \mathcal{S}\left(\prod_{i<j} F_{ij}\right)|\Phi\rangle. \tag{6}$$

In this equation, Φ is an anti-symmetrized Slater determinant, the F_{ij} are state-dependent two-body correlation operators, and $\mathcal{S}$ is a symmetrization operator. The

symmetrization operator indicates a sum over all orders of terms in the product, and is required since the correlation operators between different pairs do not commute.

For light nuclei, it suffices to choose Φ as a spin-isospin vector independent of all spatial coordinates:

$$\Phi(^2H) = \mathcal{A}[(n \uparrow)_1(p \uparrow)_2], \tag{7}$$

$$\Phi(^3H) = \mathcal{A}[(n \downarrow)_1(n \uparrow)_2(p \uparrow)_3], \tag{8}$$

$$\Phi(^4He) = \mathcal{A}[(n \downarrow)_1(n \uparrow)_2(p \downarrow)_3(p \uparrow)_4]. \tag{9}$$

In this notation, $\mathcal{A}$ is an anti-symmetrization operator indicating a sum over all possible interchanges of particles with appropriate signs. For larger nuclei (A > 4), spatial degrees of freedom must be incorporated into the Φ. Here, however, we can choose the pair correlation operators F_{ij} to give the correct asymptotic conditions on the wave function.

We choose the pair correlations to have the following form:

$$F_{ij} = f^c(r_{ij})\left[1 + \left(\sum_k u_3(r_{ij},\mathbf{R})u^k(r_{ij})O_{ij}^k\right)\right], \tag{10}$$

where the sum over operators k runs over all momentum-independent operators in the interaction (Eq. 3). The pair correlations f^c and u^k are obtained by solving two-body differential equations of the general form:[3,4]

$$[-\frac{\hbar^2}{m}\nabla^2 + v(r_{ij}) + \lambda(r_{ij})]F(r_{ij}) = 0, \tag{11}$$

where $\lambda(r)$ contains several variational parameters. In the spin singlet channels, two uncoupled equations are solved, one for T=0 and one for T=1. In the spin triplet channels, coupled equations are solved for the central and tensor correlations. Once the equations are solved in the various channels, linear combinations are obtained which can be cast in the operator form of Eq. 10.

The function $\lambda(r)$ is a woods-saxon at short distances. The width and range of the woods-saxon are variational parameters. At long distances its form is determined by requiring that the wave function have the correct asymptotic properties as one nucleon is removed from the rest. The separation energy which determines the exponential decay is an additional variational parameter, as is the ratio of the tensor and central correlations at long distance.

The u_3 correlation in Eq. 10 is a three-body term which reduces the strength of the operator-dependent two-body correlations for some configurations of the nucleons.[1] It depends not only on the pair distance r_{ij} but also on the positions of all the other particles. Empirically, it has proven useful to parametrize u_3 as

$$u_3(r_{ij},\mathbf{R}) = \prod_{k\neq i,j}\left[1 - t_1(\frac{r_{ij}}{R_{ijk}})^{t_2}\exp(-t_3R_{ijk})\right], \tag{12}$$

6

with

$$R_{ijk} = r_{ij} + r_{ik} + r_{jk}. \tag{13}$$

The values of t_1, t_2, and t_3 are determined variationally. In principle they could be adjusted independently for each pair correlation operator (each k), but in practice they are usually chosen to be the same in all channels.

The exact deuteron wave function can be cast in the form of Eq. 6. In this case the three-body correlation u_3 is replaced by the identity, and the function $\lambda(r)$ is simply a constant, the deuteron binding energy. The functions $f^c(r)$ is $u(r)$, the s-wave part of the deuteron wave function. The tensor term $f^c(r)u^S(r)$ is, within a normalization constant, $w(r)$, the d-state component of the wave function. The deuteron's wave function is worked out in the 3rd component of spin and isospin basis in the Appendix. For the deuteron, of course, the components of the wave function are only functions of one variable, so that calculating expectation values of any operator is relatively easy. For larger systems, though, this becomes progressively more difficult. Hence, we rely upon Metropolis Monte Carlo to calculate the necessary integrals.

4. Variational Monte Carlo

Given a parametrized wave function in the form of Eq. 6, $\langle H \rangle$ must be minimized as a function of the variational parameters. Evaluating $\langle H \rangle$ involves computing many 3A dimensional integrals, so we turn to Monte Carlo methods, in particular to Metropolis Monte Carlo. Monte Carlo methods in general become more valuable as the dimension of the space increases, and their efficiency depends to a great extent on the quantity to be measured and also upon the care with which they are applied.

Monte Carlo methods as applied here are described in some detail in a book by Whitlock and Kalos.[23] I can only provide some of the basics here. Those interested can consult this book and other standard references to determine optimum methods for sampling various distribution functions, and also for more detailed discussions of the Metropolis and Green's Function Monte Carlo methods. Also, R. B. Wiringa and I[4] have written a book chapter which contains quite specific discussions of the Variational Monte Carlo methods as applied to light nuclei and also includes a sample program.

A. VMC - General Method

Metropolis Monte Carlo[24] is designed to evaluate ratios of integrals such as:

$$\langle \mathcal{O} \rangle = \frac{\int W(\mathbf{R})\mathcal{O}(\mathbf{R})d\mathbf{R}}{\int W(\mathbf{R})d\mathbf{R}}, \tag{14}$$

where $W(\mathbf{R})$ is a positive definite function. While such a form may seem rather limited, in fact many interesting physics problems can be written in this way. Classical statistical mechanics is a primary example. If we take $W(\mathbf{R})$ to be $\exp(-\beta H)$ and $\mathcal{O}$

to be an observable, we can use the Metropolis method to compute the expectation value of $\mathcal{O}$ at an inverse temperature β.

Quantum variational calculations can also be performed using the Metropolis method. The standard choice is

$$W(\mathbf{R}) = \Psi_T^\dagger(\mathbf{R})\Psi_T(\mathbf{R}) \tag{15}$$

and $O(\mathbf{R})$ to be the operator acting on $\Psi_T(\mathbf{R})$ at that point:

$$O(\mathbf{R}) = \frac{\Psi_T^\dagger(\mathbf{R}) \, \mathcal{O} \, \Psi_T(\mathbf{R})}{\Psi_T^\dagger(\mathbf{R})\Psi_T(\mathbf{R})}. \tag{16}$$

The wave functions are necessary for the case when $\mathcal{O}$ depends upon momentum, and therefore includes derivative operators. For purely static scalar quantities, the wave functions will divide out in this expression. Note that I have suppressed the dependence of the trial wave function on the variational parameters $\{\alpha\}$. With this choice of W, the denominator in Eq. 14 is simply the normalization of the wave function, while the numerator gives the expectation value of the operator $\mathcal{O}$. Initially we are trying to minimize the energy in a variational calculation, so we consider the case where $\mathcal{O}$ is the Hamiltonian. In nuclear physics, the Hamiltonian (and also the wave function) will depend upon the spin and isospin of the nucleons and the functions W and O involve sums over all possible spin-isospin states. For simplicity, however, we first consider the case of a spin-isospin independent interaction where the wave function only depends upon the spatial coordinates of the particles.

The Metropolis algorithm is based upon the fact that the ratio in Eq. 14 can be evaluated as an average over a set of points $\mathbf{R}_i$ distributed with probability distribution $W(\mathbf{R})$:

$$\langle \mathcal{O} \rangle = \lim_{N \to \infty} \frac{1}{N} \sum_{i=1}^{N} \mathcal{O}(\mathbf{R}_i). \tag{17}$$

In the limit of an infinite sample of points this relation is exact, but in actual calculations there is a statistical error associated with finite sample sizes. Under very general conditions, the central limit theorem states that the statistical error will go like $1/\sqrt{N}$ for large N.

The Metropolis algorithm allows us to obtain a set of points $\mathbf{R}_i$ for an almost arbitrarily complicated function $W(\mathbf{R})$. This is important because our trial wave functions contain strong correlations, and it is difficult to perform the integrals in any other way. In essence, the Metropolis method sets up an artificial dynamics such that the equilibrium distribution of points is proportional to $W(\mathbf{R})$. The primary ingredient in the Metropolis algorithm is detailed balance, which simply requires that the net flux from any point $\mathbf{R}$ to any point $\mathbf{R}'$ must be balanced by the flux in the reverse direction when equilibrium has been reached. Clearly this is more restrictive than is absolutely necessary, nevertheless it is a very valuable technique.

A random walk algorithm can then be developed which satisfies detailed balance and gives an equilibrium distribution proportional to an arbitrary $W(\mathbf{R})$. Suppose we start at $\mathbf{R}_1$, and construct a random walk in which each step contains two elements, a proposed (trial) move and an acceptance/rejection step. First, a point $\mathbf{R}_t$ is chosen for the trial move with a transition probability $T(\mathbf{R}_1 \rightarrow \mathbf{R}_t)$, and second, this trial move is accepted with probability $A(\mathbf{R}_1 \rightarrow \mathbf{R}_t)$. If the move is accepted $\mathbf{R}_2$ is set to $\mathbf{R}_t$, otherwise $\mathbf{R}_2$ is set to $\mathbf{R}_1$. The whole process is then repeated (the next step beginning from $\mathbf{R}_2$) until the walk has reached equilibrium and a sufficient number of points have been generated to obtain accurate results.

A little thought will convince you that detailed balance imposes the following condition on the random walk if it is to generate an equilibrium distribution proportional to $W(\mathbf{R})$.

$$W(\mathbf{R}_1)T(\mathbf{R}_1 \rightarrow \mathbf{R}_2)A(\mathbf{R}_1 \rightarrow \mathbf{R}_2) = W(\mathbf{R}_2)T(\mathbf{R}_2 \rightarrow \mathbf{R}_1)A(\mathbf{R}_2 \rightarrow \mathbf{R}_1). \qquad (18)$$

The left hand side of this equation is the flux from $\mathbf{R}_1$ to $\mathbf{R}_2$, it is given by the product of the probability of being at $\mathbf{R}_1$ (which we require to be $W(\mathbf{R}_1)$), the probability T of proposing a move from $\mathbf{R}_1$ to $\mathbf{R}_2$, and the probability A of accepting that proposed move. The right hand side of the equation is the total flux in the opposite direction.

A very simple choice for $T(\mathbf{R}_i \rightarrow \mathbf{R}_t)$ is a constant $(1/L^3)$ within a 3A dimensional cube with side L. This transition probability is trivial to implement. For each component i of the 3A dimensional vector, simply take:

$$\mathbf{R}_{ti} = \mathbf{R}_{1i} + 2L(\zeta_i - 0.5), \qquad (19)$$

where the ζ_i are random numbers evenly distributed between 0 and 1. With this choice of T, it is obvious that $T(\mathbf{R}_1 \rightarrow \mathbf{R}_2)$ is identical to $T(\mathbf{R}_2 \rightarrow \mathbf{R}_1)$. If $\mathbf{R}_2$ is within the box centered at $\mathbf{R}_1$, $\mathbf{R}_2$ is also within the box centered upon $\mathbf{R}_1$ and both transition probabilities are equal, but if $\mathbf{R}_2$ is outside the box both transition probabilities are zero.

With this choice for T detailed balance becomes particularly simple. We can satisfy Eq. 18 by taking

$$A(\mathbf{R}_1 \rightarrow \mathbf{R}_2) = \min\left[1, \frac{W(\mathbf{R}_2)}{W(\mathbf{R}_1)}\right]. \qquad (20)$$

Note that the acceptance probability must always be between zero and one. If the function W is greater at the new point than at the old, the move will always be accepted. Otherwise, it will be accepted with a probability equal to the ratio of the functions. Note that a total of 3A + 1 random numbers are needed at each step in the walk, 3A to choose a trial step and one to accept or reject it.

The resulting algorithm, employing a general transition probability T, can be written down very simply:

1. Given a 3A dimensional coordinates $\mathbf{R}_i$, generate a trial coordinate point $\mathbf{R}_t$ with probability $T(\mathbf{R}_i \rightarrow \mathbf{R}_t)$.

2. Calculate the quantities $W(\mathbf{R}_1), W(\mathbf{R}_t), T(\mathbf{R}_1 \rightarrow \mathbf{R}_t)$, and $T(\mathbf{R}_t \rightarrow \mathbf{R}_1)$, the transition probability for the reverse step. The acceptance probability is given by the expression:

$$A(\mathbf{R}_1 \rightarrow \mathbf{R}_t) = \min\{1, \frac{W(\mathbf{R}_t)T(\mathbf{R}_t \rightarrow \mathbf{R}_1)}{W(\mathbf{R}_1)T(\mathbf{R}_1 \rightarrow \mathbf{R}_t)}\} \tag{21}$$

3. Accept or reject the move with probability A. If the move is accepted, set $\mathbf{R}_{i+1}$ equal to $\mathbf{R}_t$, otherwise set it to $\mathbf{R}_i$.

4. Calculate all quantities of interest (the Hamiltonian, etc.) at $\mathbf{R}_{i+1}$, adding the contributions to the average over all points (Eq. 17).

The random walk will only generate points distributed with probability $W(\mathbf{R})$ after it has reached equilibrium. Convergence to equilibrium is an important consideration that must be tested in each calculation. All results obtained prior to equilibrium should be disregarded in the averages above. This is usually not a problem in light nuclei as several hundred steps normally suffice unless one starts from a pathological initial point (one nucleon 20 fm from the others, for example). A good way to test for equilibrium is to compute the average over 'blocks' of consecutive points in the random walk consisting of several hundred points to several thousand points each.

Eventually, the averages within each block should settle down to a constant plus a (hopefully small) fluctuating term. If the blocks are large enough, the averages should have a normal distribution centered on the true mean, and the error can be estimated from them using the central limit theorem:

$$\Delta\langle\mathcal{O}\rangle \approx \sqrt{[\overline{\langle\mathcal{O}\rangle^2} - \overline{\langle\mathcal{O}\rangle}^2]/M}. \tag{22}$$

where $\Delta\langle\mathcal{O}\rangle$ is an estimate of the error in determining $\langle\mathcal{O}\rangle$ and M is the total number of blocks. The expression involves the average of the square of the estimated operator expectation value minus the square of the average, and the bars indicate averages over blocks rather than individual points. The results in each block are themselves averages over a few hundred to a few thousand points in the walk. This error estimate is only valid when the blocks are 'large enough' so that the central limit applies. The size of blocks required must be tested in each calculation, but this test involves only a re-analysis of the run. Smaller blocks can be grouped into larger ones in order to insure that the statistical error is independent of the block size.

I have not yet specified how to choose the step size L in the random walk. The choice of L strongly affects the efficiency of the calculation but should not affect the final average. For example, if L is very small then nearly all moves will be

accepted but many steps will required per block to eliminate the correlations between neighboring blocks. Similarly, if L is too large all moves are likely to be rejected, and again many steps will be required to gain independent samples. The general lore holds that adjusting L so that approximately half the moves are accepted is a reasonable choice. Numerical experiments testing the correlations between nearby points in the walk can be valuable in optimizing L.

One can also improve the efficiency by making better choices for the transition and acceptance probabilities. One popular alternative is to include information about the first derivative of W evaluated at $\mathbf{R}_1$ in the transition probability $T(\mathbf{R}_1 \rightarrow \mathbf{R}_t)$.[23] In this case the acceptance A must involve the transition probability for the reverse step, which in turn depends upon the derivative of W at $\mathbf{R}_t$. The transition probability T must be positive definite and normalized such that $\int T(\mathbf{R}_1 \rightarrow \mathbf{R}_t)d\mathbf{R}_t = 1$ for any $\mathbf{R}_1$.

Variational Monte Carlo calculations are constructed so that they will be more efficient for better trial wave functions. In fact, if the trial wave function is an exact eigenstate of the Hamiltonian the energy's statistical error will be zero. In this ideal case every sample of $H(\mathbf{R})$ (Eq. 16) will produce the same result, the ground state energy. This is not true for expectation values of other quantities. Rapidly varying functions, for example charge form factors at high momentum transfer, will have much larger statistical errors. In many cases it is possible to reduce the error by using different weight functions W, or perhaps by doing the integrals over some coordinates with traditional numerical methods rather than by Monte Carlo.

Another very useful technique is called 'reweighting'.[23] Since we are initially concerned with calculating the difference in energy between two wave functions, it is more efficient to calculate this difference directly. For example, suppose we construct an initial random walk using the square of the wave function Ψ_{T1} for the weight function $W(\mathbf{R})$. The energy of this wave function can be calculated easily from this walk, but we can also use it to evaluate the energy difference between two wave functions. The energy difference can be written in the form of Eq. 17:

$$\langle \Psi_{T1}|H|\Psi_{T1}\rangle - \langle \Psi_{T2}|H|\Psi_{T2}\rangle = \frac{\int d\mathbf{R}\frac{\Psi_{T1}H\Psi_{T1}}{W(\mathbf{R})}W(\mathbf{R})}{\int d\mathbf{R}\frac{\Psi_{T1}\Psi_{T1}}{W(\mathbf{R})}W(\mathbf{R})} - \frac{\int d\mathbf{R}\frac{\Psi_{T2}H\Psi_{T2}}{W(\mathbf{R})}W(\mathbf{R})}{\int d\mathbf{R}\frac{\Psi_{T2}\Psi_{T2}}{W(\mathbf{R})}W(\mathbf{R})} \quad (23)$$

and computed using any weight function W, in particular the square of the original wave function Ψ_{T1}. Of course, we will now have to compute both the numerator and denominator separately (the denominator in the second term is no longer exactly one at each point), but the correlations between the two calculations can be exploited to greatly reduce the statistical errors. This method is most useful when the differences between the two wave functions are not too large.

B. *VMC - Applications to Light Nuclei*

Variational Monte Carlo calculations of light nuclei[1-4] are somewhat more complicated than described above because of the spin-isospin dependence of the interaction and wave function. In this case, the expectation value of the Hamiltonian can be written:

$$\langle H \rangle = \frac{\int d\mathbf{R} \sum_{kl} \frac{\Psi_k^\dagger(\mathbf{R}) H_{kl} \Psi_l(\mathbf{R})}{W(\mathbf{R})} W(\mathbf{R})}{\int d\mathbf{R} \sum_{kl} \frac{\Psi_l^\dagger(\mathbf{R}) \Psi_l(\mathbf{R})}{W(\mathbf{R})} W(\mathbf{R})} \tag{24}$$

where the sums over k and l run over all spin-isospin states. In principle, we could use a weight function W which depends upon k and l, and perform the sums as well as the integrals by Monte Carlo. In general, though, this will produce large statistical errors since the low-variance property for the energy described above only applies to the full Hamiltonian acting on the full wave function. Therefore, we simply sum over all k and l at each point in the walk, although this places severe practical limits on the size of nucleus that can be studied.

One can choose W to be:

$$W(\mathbf{R}) = \sum_l \Psi_l^\dagger(\mathbf{R}) \Psi_l(\mathbf{R}). \tag{25}$$

In fact we use something slightly more complicated, and include a Monte Carlo sampling of the orders of pair correlation operators implied by the symmetrization operator S in the trial wave function (Eq. 6). This entails choosing a weight function which depends upon the order of operators in the left and right hand wave function, and requires a calculation of the normalization of the wave function as well as $\langle H \rangle$.[1,4] For example, in a three-body nucleus:

$$S(F_{12} F_{13} F_{23}) = \frac{1}{\sqrt{6}} [F_{12} F_{13} F_{23} + F_{13} F_{12} F_{23} + F_{23} F_{12} F_{13} + ...]. \tag{26}$$

Labeling the order of operators by p and q (and suppressing the spin-isospin indices):

$$\Psi^\dagger(\mathbf{R}) = \sum_p \Psi_p^\dagger(\mathbf{R}),$$
$$\Psi(\mathbf{R}) = \sum_q \Psi_q(\mathbf{R}), \tag{27}$$

we choose

$$W_{pq}(\mathbf{R}) = |Re\langle \Psi_p^\dagger(\mathbf{R}) | \Psi_q(\mathbf{R}) \rangle|. \tag{28}$$

In this expression I have indicated the sum over all spin-isospin states by angled brackets. Note that since the left and right hand terms are no longer simply Hermitian conjugates, the absolute magnitude is required in order to ensure that W is

12

positive definite. This also implies that one must calculate the denominator explicitly. For light nuclei, though, we have observed that the real part of the product $\langle \Psi_p^\dagger \Psi_q \rangle$ is positive for reasonable correlation functions.

Another complication arises when trying to compute the kinetic energy and the momentum-dependent terms in the interaction. Because of the complicated matrix structure of the wave function, it is very difficult to compute directly the momentum operators acting on the wave function. Consequently, all derivatives are evaluated simply by re-calculating the wave function at slightly displaced values of the particle coordinates, and forming the numerical derivatives:

$$\nabla_j^i \Psi\{\mathbf{R}\} = [\Psi\{\mathbf{R} + \epsilon \hat{r}_j^i\} - \Psi\{\mathbf{R} - \epsilon \hat{r}_j^i\}]/[2\epsilon]$$

$$\nabla_j^{i^2} \Psi\{\mathbf{R}\} = [\Psi\{\mathbf{R} + \epsilon \hat{r}_j^i\} + \Psi\{\mathbf{R} - \epsilon \hat{r}_j^i\}] - 2\Psi\{\mathbf{R}\}]/[\epsilon^2]. \quad (29)$$

In these expressions i represents a direction (x, y or z), and j represents the particle. The expectation values of L^2 terms are treated similarly, although in some cases it is more convenient to use integration by parts so that only first derivatives are required.

Typically, twenty to thirty runs are required to optimize the variational parameters. Most of the calculations are difference calculations designed to compute the energy difference of various wave functions (Eq. 23). Each run will require several thousand configurations in order to obtain a statistical accuracy of a few hundredths of an MeV. Once the optimum wave function has been determined, a set of Monte Carlo calculations should be undertaken to determine all of the expectation values. For the three-body problem, ten to twenty thousand configurations seem to provide reasonable statistical accuracy for the energy and one-body densities. Ten thousand configurations takes roughly 30 minutes of cpu time on a one megaflop computer.

Typical results for the three-body problem are given in Table I, and contrasted with the 'exact' Faddeev results. Variational results are always an upper bound to the true ground-state energy, for the triton the variational energy is typically about 0.3 - 0.6 MeV higher than the Faddeev. Wiringa[25] has recently improved the variational wave function by adding $L \cdot S_{ij}$ two-body correlations and including three-body correlations. These improvements reduce the energy difference significantly.

No upper bound property exists for operators other than the Hamiltonian, however. In fact, while the error in energy is second order in the error in the trial wave function, the error in other observables is generally first order. Consequently, two variational wave functions may give very similar energies but different values of other observables. For example, the point rms radius of the nucleons can change by 0.05 to 0.1 fm without significantly affecting the ground state energy. This uncertainty in the wave function, rather than the statistical error associated with the Monte Carlo integrations, is often the most important difficulty with variational calculations. Comparisons with other quantities such as the magnetic form factors (discussed in section 6) indicate that the variational wave functions provide a good overall description of the structure of light nuclei. Nevertheless, methods to systematically improve the variational wave function are extremely valuable.

13

Table 1: Triton Results - Variational and Faddeev

Interaction	Method	Energy (MeV)		$\langle r_i^2 \rangle^{1/2}$ (fm)		% (S=3/2)	
AV14 + TNI	Variational	-8.42	(04)	1.68	(02)	9.9	(1)
AV14 + TNI	Faddeev	-8.99		1.65		10.0	
Nijmegen	Variational	-7.25	(03)	1.86	(03)	7.7	(1)
Nijmegen	Faddeev	-7.63		1.77		7.9	
Reid V8	Variational	-7.08	(05)	1.82	(02)	-	
Reid V8	Faddeev	-7.59		1.76		9.7	

Summary of triton results from reference 26. Energies are given in MeV, distances in fm, and statistical errors are indicated in parentheses. The rms radii given are point nucleon radii. The last column gives the magnitude of the spin 3/2 wave function component; except for very small P-state components this is equal to the D-state percentage.

5. Green's Function Monte Carlo

Green's Function Monte Carlo (GFMC) calculations project an exact ground or low-lying state wave function Ψ_0 from an initial trial wave function Ψ_T. Monte Carlo techniques are used to calculate the operator $\exp(-H\tau)$ acting on Ψ_T for large imaginary times τ. Expanding a variational wave function $\Psi_T\{\alpha\}$ in eigenstates of H

$$\Psi_T\{\alpha\} = \sum_m \beta_m\{\alpha\}\Psi_m \tag{30}$$

we find

$$\exp(-H\tau)\Psi_T\{\alpha\} = \sum_m \exp(-E_n\tau)\beta_m\{\alpha\}\Psi_m, \tag{31}$$

where I have included $\{\alpha\}$ to label the implicit dependence of Ψ_T on its variational parameters. For large τ, only the state with the lowest energy eigenvalue will survive. You should be aware that many similar algorithms are available that go under different names, including Green's Function Monte Carlo (GFMC),[5-7] Diffusion Monte Carlo (DMC),[27] etc. I will not go into the distinctions here, but one should be aware of their existence. Most of these algorithms are primarily designed to treat systems without state-dependent interactions, limiting their applicability to nuclear physics.

A. *GFMC - General Method*

All of the methods are based upon high-temperature or short-time expansions of the Green's Function:

$$\exp(-H\tau) = \prod \exp(-H\Delta\tau) \tag{32}$$

where the product runs over many short time steps $\Delta\tau$.

Of course we do not know even the short-time propagator exactly; the exact form would require imply a knowledge of all eigenstates. However, for short time steps $\Delta\tau$ we can construct accurate approximations to the propagator. The simplest approximation is:

$$
\begin{aligned}
G(\mathbf{R}',\mathbf{R}) &= \langle\mathbf{R}'|\exp(-H\Delta\tau)|\mathbf{R}\rangle \\
&\approx \exp(-V(\mathbf{R})\Delta\tau/2)\langle\mathbf{R}'|\exp(-T\Delta\tau)|\mathbf{R}\rangle\exp(-V(\mathbf{R}')\Delta\tau/2),
\end{aligned} \quad (33)
$$

where I have split the Hamiltonian into its kinetic (T) and potential (V) pieces and assumed that the potential is local.

Green's Function Monte Carlo is similar in many respects to a transport Monte Carlo simulation. The basic idea is choose an initial set of configurations with density proportional to a trial wave function, and to use Monte Carlo methods to iterate an integral equation:

$$
\Psi^{i+1}(\mathbf{R}') = \int d\mathbf{R}\, G(\mathbf{R}',\mathbf{R})\Psi^i(\mathbf{R}) \quad (34)
$$

until convergence to the ground state wave function. Each configuration is an independent copy of the entire system, and their 'trajectories' are followed as Eq. 34 is iterated. The kinetic energy term allows the sampled points to move about in configuration space while the potential energy duplicates or destroys walks.

The Monte Carlo simulation mimics a diffusion process in which the kinetic energy term governs the rate of the diffusion, since:

$$
\langle\mathbf{R}'|\exp(-T\Delta\tau)|\mathbf{R}\rangle = N\exp\left[\frac{-(\mathbf{R}-\mathbf{R}')^2}{4\frac{\hbar^2}{2m}\Delta\tau}\right], \quad (35)
$$

where N is a normalization constant that insures $\int d\mathbf{R}'\langle\mathbf{R}'|\exp(-T\Delta\tau)|\mathbf{R}\rangle = 1$. The potential, on the other hand, can be thought of as a source or sink of random walks. When the potential is repulsive, the Green's function (Eq. 33) is small and walks will be absorbed. In regions where the potential is attractive, though, new walks will be created.

For state-independent interactions it is not necessary to use short-time approximation (Eq. 33). Domain GFMC methods[7] exploit an integral equation for the inverse of the Hamiltonian, locally expanding this true Green's function about a constant-potential Green's functions within a domain. It is possible to use Monte Carlo techniques to perform one random walk within another, sampling the exact Green's function and hence avoiding any short-time approximation. Generalizations of the exact method to state-dependent potentials or momentum-dependent interactions is an unsolved problem, however. Consequently, we will employ methods that, although somewhat more sophisticated than Eq. 33, do include a time-step error. This time step error can be made arbitrarily small by making $\Delta\tau$ very small. The errors per time step in this short-time approximation above are proportional to $\Delta\tau^2$,

as you can see by expanding the exponentials. However, the overall error is proportional to $\Delta\tau$, as the total number of steps required to propagate a given imaginary time is proportional to $1/\Delta\tau$.

GFMC methods are closely related to the finite-temperature simulations in condensed matter (Path Integral[28] and Fermion Monte Carlo[30]) and lattice QCD. These methods retain the complete history of the system over time (its world-line or path), and evaluate

$$\langle\mathcal{O}\rangle = \frac{\sum_{\mathbf{R}}\langle\mathbf{R}\mathcal{O}\exp(-\beta H)\mathbf{R}\rangle}{\sum_{\mathbf{R}}\langle\mathbf{R}\exp(-\beta H)\mathbf{R}\rangle}. \tag{36}$$

to determine the expectation value of an operator $\mathcal{O}$ at an inverse temperature β. Clearly, this expression is of the form of Eq. 14, and can be evaluated using Metropolis Monte Carlo to sample over all paths. Note that the paths are closed since they begin and end at the same point $\mathbf{R}$. The fact that the complete 'time' history must be retained typically limits these methods to $\approx 50-100$ steps in inverse temperature.

Here, however, we are particularly interested in projecting out specific quantum states. We can use this to our advantage and build in our knowledge of the approximate eigenstates. The basic technique is called 'importance sampling.' Multiplying and dividing Eq. 34 by an importance function Ψ_I, we obtain

$$\Psi_I(\mathbf{R}')\Psi^{i+1}(\mathbf{R}') = \int d\mathbf{R}\left[\Psi_I(\mathbf{R}')G(\mathbf{R}',\mathbf{R})\frac{1}{\Psi_I(\mathbf{R})}\right]\Psi_I(\mathbf{R})\Psi^i(\mathbf{R}), \tag{37}$$

where the quantity in brackets is designated the importance sampled Green's function. For bosonic systems, Ψ_I is usually the optimum trial wave function Ψ_T obtained in a variational calculation. This construction has the advantage that the energy can be obtained as an average of $\Psi_T^\dagger H\Psi_T/\Psi_T^\dagger\Psi_T$, and consequently there is no statistical error in the limit that the trial state is equal to the exact one. Also, using the spectral representation of the Green's function we can compute the total number of samples $I(\mathbf{R})$ generated by a point originally at $\mathbf{R}$:

$$I(\mathbf{R}) = \int d\mathbf{R}'\left[\Psi_I(\mathbf{R}')\sum_m\Psi_m(\mathbf{R}')\exp(-E_M\Delta\tau)\Psi_m(\mathbf{R})\frac{1}{\Psi_I(\mathbf{R})}\right]. \tag{38}$$

In the limit that Ψ_I is equal to the ground state (and $E_0 = 0$), $I(\mathbf{R})$ is precisely one independent of the starting point $\mathbf{R}$. Good choices for Ψ_I imply that each configuration in the i'th generation will contribute almost exactly one configuration to generation i+1. This limitation of fluctuations is very important in reducing the statistical bias of the calculation.

At this stage, it is also useful to consider better approximations to the Green's function than Eq. 33. For static (momentum-independent) potentials, it is useful to construct

$$G(\mathbf{R}',\mathbf{R}) \approx G_0(\mathbf{R}',\mathbf{R})\prod_{i<j}\frac{g_{ij}(\mathbf{r}_{ij},\mathbf{r}'_{ij})}{g_{ij}^0(\mathbf{r}_{ij},\mathbf{r}'_{ij})}, \tag{39}$$

16

where G_0 is the free-particle propagator for the A-body system, g_{ij} is the two-body propagator including the interaction, and g_{ij}^0 is the two-body free propagator. The free particle propagators are just normalized gaussians:

$$G_0(\mathbf{R}', \mathbf{R}) = N \exp[\frac{-(\mathbf{R}' - \mathbf{R})^2}{4\Delta\tau\hbar^2/(2m)}]$$

$$g_{ij}^0(\mathbf{r}'_{ij}, \mathbf{r}_{ij}) = N' \exp[\frac{-(\mathbf{r}'_{ij} - \mathbf{r}_{ij})^2}{4\Delta\tau\hbar^2/(2\mu)}]. \tag{40}$$

The lowest order approximation to the ratio of two-body propagators recovers Eq. 33. The exact two-body Green's function, though, can be evaluated as an average over all gaussian paths linking $\mathbf{r}_{ij}$ and $\mathbf{r}'_{ij}$. In finite-temperature studies of bulk liquid helium, Ceperley and Pollock[28,29] have used this method to determine the Green's function of Eq. 39.

The simplest feasible GFMC algorithm can be described as follows:

1. Begin with a set of points in configuration space distributed with probability density $\Psi_I\Psi'$. At the zeroth iteration, Ψ^0 is the trial wave function Ψ_T (here assumed to be the same as Ψ_I), so the original set of points can be generated with the Metropolis methods described previously.

2. For each point in the i'th generation $\mathbf{R}$, generate a new point $\mathbf{R}'$ in the 3A dimensional space by sampling from a normalized approximate Green's function $\tilde{G}(\mathbf{R}, \mathbf{R}')$. In the simplest case, $\tilde{G}$ can be taken to be the free particle Green's function. A better choice, though, is to include some information about the importance function, for example by including the first derivative of $\Psi_I(\mathbf{R})$ in $\tilde{G}$.

3. Assign each configuration a weight equal to the ratio of the true importance sampled Green's function to the approximate Green's function $\tilde{G}$. This ratio is given by (Eq. 39):

$$w_i = \frac{\Psi_I(\mathbf{R}')}{\Psi_I(\mathbf{R})} \frac{G_0(\mathbf{R}', \mathbf{R})}{\tilde{G}(\mathbf{R}', \mathbf{R})} \prod_{i<j} \frac{g_{ij}(\mathbf{r}_{ij}, \mathbf{r}'_{ij})}{g_{ij}^0(\mathbf{r}_{ij}, \mathbf{r}'_{ij})} \tag{41}$$

4. Compute all quantities of interest at the location $\mathbf{R}'$, and include them in a weighted average over all points. For example, the energy at generation i can be evaluated as:

$$\sum_i w_i \frac{\Psi_T^\dagger(\mathbf{R}'_i)H\Psi_T(\mathbf{R}'_i)}{\Psi_T^\dagger(\mathbf{R}'_i)\Psi_T(\mathbf{R}'_i)} \tag{42}$$

for the case $\Psi_I = \Psi_T$. In the more general case, both the numerator

$$N = \sum_i w_i \left[\frac{\Psi_T^\dagger(\mathbf{R}'_i)H\Psi_T(\mathbf{R}'_i)}{\Psi_T^\dagger(\mathbf{R}'_i)\Psi_T(\mathbf{R}'_i)} \right] \left[\frac{\Psi_T(\mathbf{R}'_i)}{\Psi_I(\mathbf{R}'_i)} \right] \tag{43}$$

17

and denominator

$$D = \sum_i w_i \frac{\Psi_T(\mathbf{R}'_i)}{\Psi_I(\mathbf{R}'_i)} \tag{44}$$

must be evaluated, and the energy is N/D.

5. Each weighted configuration is replaced by n copies of the configuration with unit weight, n being chosen to replicate on average the original weight w_i. For example, if w_i is 0.5, choose n to be 1 half the time and 0 half the time; if w_i is 2.1, keep two copies with 90 % probability and three copies with 10 % probability.

Steps 2 through 5 are then repeated until convergence, each repetition representing one iteration of Eq. 37. A constant can be added to the Hamiltonian to control the growth or decrease of the population size. If this constant is such that the ground state energy is precisely zero, the population will remain constant on average. One almost never knows the exact energy initially, but the constant can be adjusted as the calculation proceeds. The growth estimate of the energy can be calculated as the logarithm of the ratio of population sizes divided by the time step $\Delta\tau$ since the ground state eventually dominates Eq. 31. In fact, this provides a very important consistency check on the calculation. The energy as determined by the growth of the population should be consistent with that determined by averaging over the individual points, as in step 4 above.

It isn't immediately obvious that the branching step above is necessary. Indeed, the results obtained by merely retaining the weight factors would be identical, on average, to those obtained with branching. However, the branching process greatly reduces the statistical error. After many generations without branching the weights of a few configurations will become much larger than the rest, and most of the computer time will be spent calculating quantities that have very low weights. Consequently, such a calculation will be very inefficient.

As I have mentioned, Green's Function Monte Carlo algorithms can be constructed which eliminate all short time approximations. Such algorithms are somewhat more complicated but have proven to be extremely valuable in condensed matter physics, where they have been used to determine the ground state energy of bulk ^{4}He as a function of the density.[10] Some analogies can be made which connect helium atoms to nuclear physics, as the helium-helium potential is very repulsive at short distances (due to the Pauli principle) and weakly attractive at large distances. The GFMC and experimental zero-temperature equations of state agree within approximately 0.1 K over a wide range of densities encompassing both the liquid and solid regions. Helium is an extremely strongly interacting quantum system; and the agreement of the many-body calculations with experimental results is very impressive. Such calculations typically employ 50 to 150 atoms confined within a periodic box. Other quantities, such as the structure function S(k), have also been computed and excellent agreement between theoretical and experimental results is achieved.

18

We now turn to fermion problems, which are considerably more difficult. In the preceding discussions, I have implicitly assumed that the wave function is positive definite. The ground state wave function of a fermion system, however, necessarily involves both positive and negative regions because it must be anti-symmetric. In some lattice problems, notably lattice QCD at zero baryon density and electronic lattice problems at half filling, the fermion problem can be overcome by introducing auxiliary fields which transform the problem into a bosonic equivalent.[30] Here I will concern myself only with continuum problems, however. Naively, the anti-symmetry can be treated by writing the wave function as the difference of two functions, each of which is positive definite:

$$\Psi^i = \Psi^{+i} - \Psi^{-i}. \tag{45}$$

Equation 34 can then be used to iterate each of the two components separately, and the results combined to determine the fermion ground state. When determining the expectation values, we will always take the overlap with an anti-symmetric trial function, hence eliminating any bosonic components in the calculation. The lowest-energy state obtained after many iterations will be the fermion ground state.
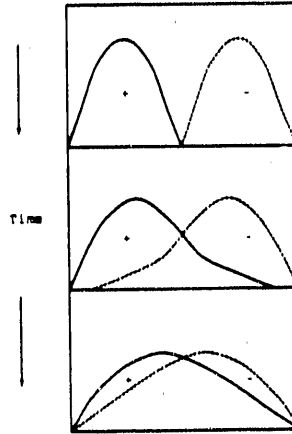

Figure 2) Transient estimation GFMC for the lowest anti-symmetric state in a 1-dimensional infinite square well. The anti-symmetric wave function is given by the difference between Ψ^+ (solid line) and Ψ^- (dashed line).

The fallacy in this simple approach is illustrated in Figure 2. Although the difference between the positive and negative distributions is, in fact, anti-symmetric, this anti-symmetric signal is completely dominated by statistical noise in the limit of many iterations (large τ). In the figure, we consider solving for the lowest-energy excitation of a one-dimensional infinite square well. The two curves indicate the density distribution of the positive and negative configurations. The top portion of the figure presents the initial distribution. The two components Ψ^+ and Ψ^- are

well-separated since they are taken from the positive and negative regions of a trial wave function. As the calculation proceeds (middle figure), the two distributions begin to overlap as they diffuse throughout the box. The signal we are interested in is the anti-symmetric wave function, here represented by the difference in the two curves.

As the iterations proceed, the relative size of this signal (bottom figure) becomes smaller and smaller, eventually being completely dominated by statistical noise. The bosonic ground state is always lower than the fermion state for spin-independent potentials, hence the growth in statistical error as the calculation proceeds. This growth arises because any bosonic signal which is introduced through statistical fluctuations increases at a faster rate than the fermion components of the wave function.

For at least a few iterations, one can allow the population size in the GFMC calculation to grow sufficiently to overcome this difficulty. This method is termed 'transient estimation'[31] and is very successful for some quantum systems, for example in studies of the electron gas[32] and liquid ^{3}He.[31,33] It is possible to prove that you can obtain a series of decreasing upper bounds to the exact ground state energy, simply by projecting out the anti-symmetric signal for as long as possible. The value of this method depends upon the accuracy of the initial trial wave function and upon the difference in energy between the lowest symmetric and anti-symmetric solutions of the Hamiltonian. The computer time required grows exponentially with the number of iterations, however, so it is not always practical to obtain a converged result.

Another variational method is also commonly used for fermion systems, the so-called 'fixed-node' method.[13,11] In this case one defines two separate regions of configuration space, one for the positive configurations (those associated with Ψ^+), and one for the negative. The positive configurations are not allowed to diffuse into the negative region and the negative configurations cannot diffuse into the positive region. Separating the system this way is equivalent to solving for a modified Hamiltonian in which an infinite barrier exists along the nodal surface. This modified Hamiltonian essentially turns the system into an approximately equivalent bosonic problem which may be solved without difficulty with GFMC.

The solution is only approximate because of the possible discontinuities in the derivative of the wave function at the nodal surface. If the nodal surface is known exactly, the fixed-node solution will yield the exact fermion ground state. However, the exact nodal surface is usually only known in one-dimensional problems like the square-well example above. In one dimension, the wave function is zero whenever two fermions are at the same point, but in many dimensions this condition is insufficient to completely determine the 3A-1 dimensional nodal surface. Nevertheless, very accurate upper bounds to the ground state energy can often be obtained with the fixed-node method. The nodal surface is usually taken from the most accurate available variational wave function.

A system of strongly interacting ^{3}He atoms provides a good test case for Monte

Carlo algorithms. By employing periodic boundary conditions with different box sizes, one can simulate an infinite system of atoms and determine the ground state energy as a function of density. An atom-atom interaction model has been developed by Aziz,[34] which consists of a strongly repulsive core region and a weakly attractive tail. The repulsive core arises from the fermi repulsion of the electrons in the atom, and the attractive tail is a result of electron re-arrangements and is dominated at long distance by the atom's induced dipole moments.

The figure below compares the results of Variational and Green's Function Monte Carlo calculations with the experimental equation of state.[11,33] As can be seen in the figure, the agreement between GFMC and experiment is excellent; the two curves are within approximately 0.1 K at all densities. The variational results are higher than the GFMC by ~ 0.3 K. It is difficult to go beyond an accuracy of ~ 0.1 K in these calculations, because at this level finite-size effects and three-atom forces become important.
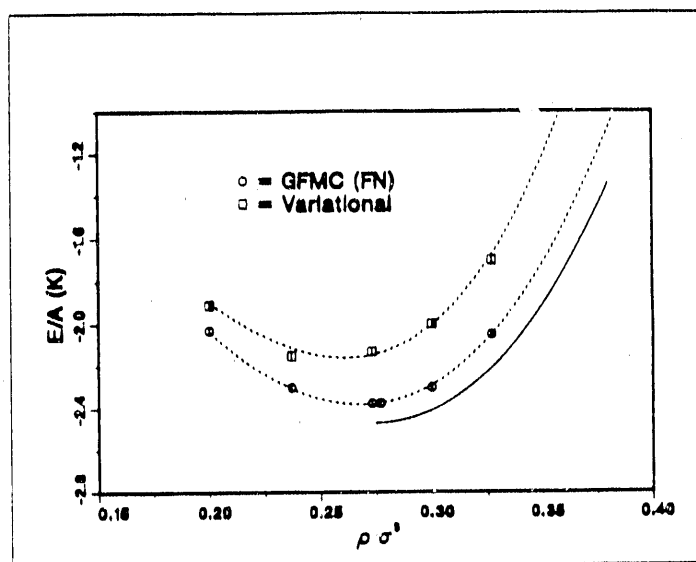

Figure 3) Ground state energy per atom versus density for liquid ^{3}He. The squares indicate variational Monte Carlo calculations, the circles fixed-node GFMC, and the solid line the experimental results.

At the equilibrium density, a transient estimation calculation has also been performed. It yields an upper bound for the ground state energy of -2.44 ± 0.04 K, which is within statistical errors of the experimental -2.47 K. We can also compare the two-body distribution function $g(r)$ that is measured in neutron and X-ray scattering experiments. The calculated curves are compared to experimental results in Figure 4. Since this is an infinite liquid, g(r) goes to one at large distances. At small distances there is a large hole in the distribution function due to the strong core repulsion. The theory and experiment agree very well, although there are slight differences at separations where finite size effects may be important.
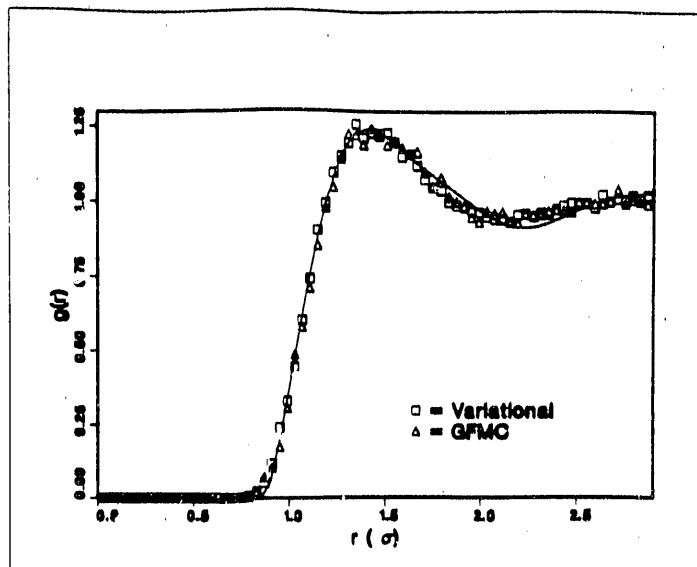
Figure 4) Two-body distribution function g(r) for liquid ^{3}He at experimental equilibrium density. The statistical errors in the Monte Carlo calculation are roughly indicated by the size of the symbols.

The GFMC calculations for bulk ^{3}He employ 54 particles with periodic boundary conditions. This is exactly the type of thing we would like to do in nuclear physics. The equation of state of nuclear matter (even at zero temperature) is a very important quantity, as are measurements of two-body distribution functions. Due to the complexities of the nuclear interaction, though, we are currently limited to studying very light nuclei. GFMC calculations with state-dependent interactions are described in the next section.

B. *GFMC - Applications to Light Nuclei*

The primary complication that arises in nuclear physics GFMC calculations is the state-dependence of the interaction. The potential, and hence the pair Green's functions (Eq. 39), are operators in spin-isospin space. Consequently, we must employ generalizations of the previous schemes to perform a Green's function Monte Carlo calculation. For example, importance sampling is more complicated since the wave function is not a simple number. In addition, the weights in general will not be a single number (or even necessarily real), so branching techniques must be modified.

Explicitly evaluating even the pair Green's function is a rather daunting task given the fact that it depends upon so many variables. In addition, the potentials between different pairs do not commute, so the pair approximation itself breaks down much more rapidly in nuclear physics than in condensed-matter problems. For these reasons, we construct approximate pair propagators by constructing 'sub-paths' between r_{ij} and r'_{ij} to evaluate $g_{ij}(r_{ij}, r'_{ij})$. These sub-paths are simply gaussian paths

22

with fixed end-points, a particular path through points r_{ij}^1, r_{ij}^2, etc. has a probability proportional to:

$$P(\mathbf{r}_{ij}^1, \mathbf{r}_{ij}^2, .. \mathbf{r}_{ij}^{N-1}) \propto \prod_{k=0}^{N-1} \exp\left[-\frac{(\mathbf{r}_{ij}^k - \mathbf{r}_{ij}^{k+1})^2}{4\hbar^2 \Delta\tau/(2\mu N)}\right],$$ (46)

where r_{ij}^0 is the fixed initial point and r_{ij}^N is the fixed endpoint. In the limit N=1 we get the original short-time approximation (Eq. 33), and in the limit $N \to \infty$ we can reconstruct the complete pair approximation (Eq. 39). When N is a power of two the path can be easily reconstructed by successive divisions, first sampling $r^{N/2}$ and then subdividing between $r^{N/2}$ and the endpoints, etc. We typically use $N = 8$, which is a compromise between accuracy and efficiency in calculating the pair propagator. We also sample several paths between r_{ij} and r'_{ij}, incorporating antithetic sampling techniques[23] to reduce the variance.

At this stage there doesn't appear to be much logic in using sub-paths since we could obtain the same effect by simply using a smaller time step in the original equations. The operator algebra enables much greater efficiency, however, when we consider only one pair of particles at a time. If we fix the positions of the particles, the momentum-independent operators in the interaction form a closed set and we can trivially exponentiate the potential.[35] The ratio of true to free particle pair Green's functions (Eq. 39) is approximated as:

$$\frac{g_{ij}(\mathbf{r}_{ij}, \mathbf{r}'_{ij})}{g_{ij}^0(\mathbf{r}_{ij}, \mathbf{r}'_{ij})} \approx \exp[\frac{-V(\mathbf{r}_{ij}^0)\Delta\tau}{2N}] \left\{ \prod_{k=1}^{N-1} \exp\left[\frac{-V(\mathbf{r}_{ij}^k)\Delta\tau}{N}\right] \right\} \exp[\frac{-V(\mathbf{r}_{ij}^N)\Delta\tau}{2N}].$$ (47)

The operator algebra given in reference 35 can then be employed to approximate this ratio in terms of the six operators

$$O_{ij}^k = \{1, \sigma_i \cdot \sigma_j, \tau_i \cdot \tau_j, \sigma_i \cdot \sigma_j \tau_i \cdot \tau_j, S_{ij}, S_{ij}\tau_i \cdot \tau_j\}$$ (48)

and associated coefficients. In forming the full A-body Green's function (Eq. 39), we use a Monte Carlo sampling to symmetrize over the order of pair Green's functions.

The nuclear interaction also contains three-nucleon and momentum-dependent two nucleon interactions. These interactions are relatively weak, hence the following generalization of Eq. 39 can be employed:

$$G(\mathbf{R}', \mathbf{R}) \approx [1 - \sum_{i<j<k} \Delta\tau V_{ijk}] \left[\prod_{i<j}[1 - \Delta\tau V_{ij}^{L\cdot S} L \cdot S_{ij}]G_0(\mathbf{R}', \mathbf{R}) \right] \prod_{i<j} \frac{g_{ij}(\mathbf{r}_{ij}, \mathbf{r}'_{ij})}{g_{ij}^0(\mathbf{r}_{ij}, \mathbf{r}'_{ij})},$$ (49)

The derivative operators in the $L \cdot S_{ij}$ operator act only on the free-particle Green's function. More accurate expressions for G are possible but difficult to implement. For example, exponentiating the two-pion-exchange three-nucleon interaction involves a complicated spin-isospin structure.

23

The remaining non-local terms are proportional to the square of the momentum operator, and hence can be described in this method as a direction-dependent 'effective mass'.[36] However, the fact that this effective mass depends upon spin and isospin limits our ability to do GFMC calculations, since the basis of the method is that the Green's function can be written as a free-particle Green's function times small corrections (of the order of $\Delta\tau$). This is no longer true for terms such as L^2 and $L \cdot S^2$, hence we solve for a simplified Argonne V8 model in which no such terms are present. The Argonne V8 model is constructed to reproduce the deuteron exactly, and to reproduce the full S- and P-wave interaction with the exception of the coupling of P and F waves. The difference between the full interaction model and the simplified V8 model can then be computed in perturbation theory. This perturbative effect is fairly small, approximately 0.15 MeV in the triton and 0.9 MeV in the alpha particle. Improved methods for treating state-dependent non-local interactions would be extremely valuable.

The basic GFMC algorithm described previously now goes through with a few fairly straightforward generalizations. Each configuration now consists not only of the coordinates of the particles, but also a set of amplitudes in the various spin-isospin channels. The amplitudes are products of the hermitian conjugate of the trial wave function times the amplitude of the true wave function. At each iteration, we first divide each amplitude by the hermitian conjugate of Ψ_T, hence reconstructing the wave function. Then we construct an approximate spin-independent Green's function $\tilde{G}$ and sample a new point $\mathbf{R}'$ from $\tilde{G}(\mathbf{R}', \mathbf{R})$. One alternative is to choose $\tilde{G}$ to be the the free A-body propagator times the ratio of central correlations in the trial wave function at the points $\mathbf{R}'$ and $\mathbf{R}$. This choice incorporates an approximate importance sampling.

Given the initial and final points in configuration space, we then construct the full Green's function in operator form, and calculate its effect acting upon the wave function at the initial point. Finally, we multiply each component of the wave function by the hermitian conjugate of the trial function's component at the new point. This completes one iteration of the Green's function equation. Branching is incorporated by using the absolute value of the sum of all amplitudes in the various channels.

Within each run we iterate approximately 1000 configurations for several hundred to a thousand generations. Approximately twenty runs are required to accurately assess the statistical errors, so the calculations are quite computer intensive. The alpha particle calculations typically require 50 - 100 hours of cpu time on a Cray-XMP. It may be possible to speed them up by incorporating better approximations to the A-particle Greens function, and hence allowing larger time steps and fewer iterations. The results obtained to date with both Variational and Green's function Monte Carlo methods are presented in the next section.

6. Results

I will first present results from a new set of GFMC calculations for the alpha particle with a three-nucleon-interaction (TNI).[37,38] The convergence of the GFMC calculation is demonstrated in figure 5, which shows the energy plotted as a function of the total iteration time τ (Eq. 31). At $\tau = 0$, the energy is equal to the variational result, and it quickly drops to the exact ground state energy. In fact, the plot covers only the initial part of the calculation, up to a total iteration time of 0.012 MeV^{-1}. The actual calculation includes 5 times as many iterations, the horizontal lines in the figure are statistical error bounds obtained by averaging the results between 0.024 and 0.060 MeV^{-1}. The convergence of the GFMC solution is determined by the accuracy of the trial wave function as well as the excitation structure of the nucleus. In this case the variational wave function seems to contain small components of high energy (short-ranged) excitations, excitations which are rapidly projected out in the GFMC method.
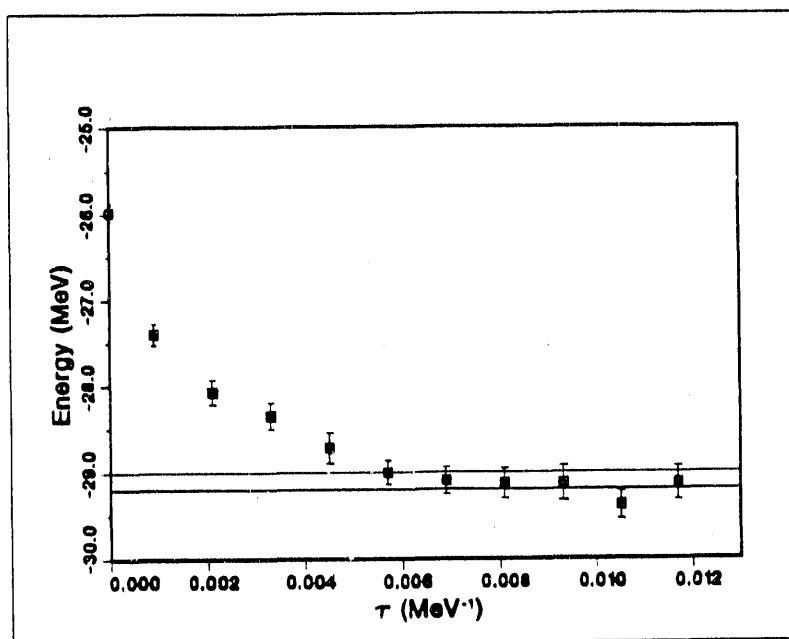

Figure 5) Alpha Particle Ground State Energy vs. iteration time τ.

The variational wave function used in this calculation was taken from reference 26 and was optimized for the Argonne V14 plus Urbana model 7 TNI. Consequently, it does not provide a very good estimate for the ground state energy with the model 8 TNI, which has a stronger repulsive component and a weaker two-pion-exchange term. However, the rms radius of this trial wave function is very near the exact result, hence it requires smaller extrapolations for the estimates of other properties. GFMC produces a wave function only in a statistical sense, and therefore ground

state energy expectation values other than the energy are extrapolated from 'mixed' and variational estimates via:

$$\langle \Psi_0 | H | \Psi_0 \rangle \approx 2\langle \Psi_T | H | \Psi_0 \rangle - \langle \Psi_T | O | \Psi_T \rangle. \tag{50}$$

The extrapolations required with the present variational wave function are generally quite small.

The three-nucleon-interaction included in these calculations is the Argonne model 8.[37] At long distances, the operator structure of this interaction is assumed to be that of the two-pion-exchange TNI (Fig. 6). In this diagram, one nucleon is excited through pion exchange to a delta resonance, which then decays by exchanging a pion with a third nucleon. Such a diagram is clearly not included in any iteration of two-body terms, and consequently must be represented, if we restrict ourselves to nucleon degrees of freedom, as a three-body force. The Urbana TNI has the form:[2]

$$V_{ijk} = U_0 \sum_{cyc} W_{2\pi}(r_{ij}) W_{2\pi}(r_{ik}) + A_0 \sum_{cyc} V_{2\pi}(\mathbf{r}_{ij}, \mathbf{r}_{ik}). \tag{51}$$

In addition to the two-pion-exchange TNI, the Urbana model contains a short-range repulsive term proportional to U_0. This term has the range of a two pion exchange on each leg, and can be motivated through dispersive corrections in the three-nucleon system. The interaction model also gives reasonable predictions for nuclear matter saturation properties in variational integral equation studies.[39]
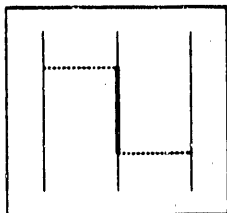

Figure 6) Two-pion-exchange three nucleon interaction. The dashed lines represent exchanged pions, the heavy solid line a delta resonance, and the thin solid lines represent nucleons.

There are, of course, many diagrams that can contribute to the TNI, making it extremely difficult to derive the three-body force in any fundamental way. Consequently, we adopt a phenomenological approach similar to that used to construct the intermediate- and short-ranged part of the NN force, and adjust the TNI's strength to fit the three-body binding energy. The parameters obtained are in rough agreement with expectations obtained by estimating the strength of two-pion-exchange diagrams such as Figure 6. I would remind you that the three-body force is quite small compared to the two-nucleon interaction, but the full TNI provides 4-5 MeV of the 28 MeV total binding in the alpha particle.

We obtain a ground state energy of -29.20 ± 0.15 MeV for the Argonne V8 + TNI model 8 interaction, approximately one MeV overbound compared to the experimental -28.3 MeV. Employing perturbation theory to estimate the difference between the Argonne V14 NN interaction and the V8 model yields 0.9 MeV repulsion, yielding a total energy of -28.3 $\pm$ 0.2 MeV, in remarkably good agreement with the experimental result. One should be somewhat cautious because of our use of perturbation theory in the difference between the V14 and V8 models; but it appears that the same three body force can be used to produce very accurate binding energies for three and four body nuclei. The Urbana TNI model 8 has been chosen to provide a good fit to the triton binding energy,[40] Faddeev results give -8.45 compared to the experimental -8.48 MeV. We have also attempted to check our perturbative estimate using three-body nuclei, perturbation theory yields very good results but the difference between V8 and V14 models is only 0.15 MeV for A=3. The expectation value of the three nucleon interaction is a small fraction ($\leq 5\%$) of the total potential energy, so at this level there is no apparent reason to introduce four- or higher-body interaction terms. Other models (Reid, Nijmegen, ...) of the NN potential give a similar underbinding for the three- and four-body nuclei, hence it should be possible to fit the binding energies of these nuclei as well with an appropriate TNI model.

The most accurate variational calculations to date[25] underestimate the alpha particle binding by approximately one MeV. As always, the total binding energy results from a sensitive cancellation between kinetic and potential terms. Each of these terms is on the order of 100 MeV (Table 2), hence the TNI represents $\sim$ 5% of the two-body potential energy, but a large fraction of the binding energy. Consequently, accurate calculations are very important when studying the effects of the three-nucleon interaction. We also present several other expectation values in Table 2. Although these numbers are not directly accessible experimentally, they do provide a useful guide to understanding light nuclei.

Table 2: Alpha Particle Expectation Values

Energy (MeV)	-28.3	(0.2)
$\langle T \rangle$	109.3	(1.2)
$\langle V_{NN} \rangle$	-136.5	(1.5)
$\langle V_\pi \rangle$	-111.8	(1.0)
$\langle V_I \rangle$	-252.5	(2.5)
$\langle V_s \rangle$	228.2	(2.1)
$\langle V_{coul} \rangle$	0.75	(0.01)
$\langle V_{3-s} \rangle$	5.0	(0.2)
$\langle V_{3-2\pi} \rangle$	-10.8	(0.2)
$\langle r_i^2 \rangle^{1/2}(fm)$	1.45	(0.01)

Of particular interest is the strong effect of the tensor interaction in the alpha particle. With the Argonne NN interaction, the tensor components contribute approximately 2/3 of the two-body potential energy in the alpha particle. Almost exactly the same fraction is found in Faddeev calculations of three-body nuclei and in cluster Monte Carlo calculations of ^{16}O.[41] The entry V_π in the table gives the contribution of the full one-pion-exchange term in the AV14 interaction, it is almost equal to the total V_{NN} expectation value. The Argonne NN interaction can be written as a sum of one-pion exchange, short range, and intermediate (two-pion) range terms. As shown in the table, there is a strong cancellation between the intermediate range attraction V_I and the short-range repulsion V_s in the two-body interaction.

Another measure of the strength of the tensor interaction is the D state probability in the four-nucleon ground state. With the Argonne plus Urbana model 8 TNI interaction, the D-state probability is 16%, other models range from 12 to 17 %. These probabilities are nearly consistent with what one would expect based upon the number of triplet pairs in the A=2, 3, and 4 body nuclei; a ratio of 1:1.5:3. In addition, the asymptotic D to S state ratio of the alpha particle wave function is in good agreement with experimental results.[3] The remainder of the wave function is dominated by the fully symmetric S-wave state, which has a probability of 82.8(0.2)%. In addition, there are small components of other symmetries, either S- or P-wave.
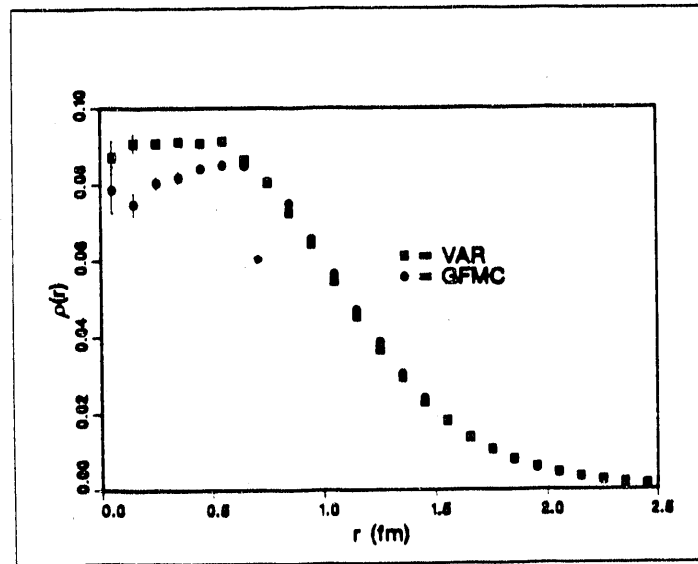

Figure 7) VMC and GFMC results for the proton density in the alpha particle.

We have also computed the proton density for both the variational and GFMC wave functions (Fig. 7). The two distributions give nearly the same rms radius and are nearly equal overall. There is a small difference within 0.5 fm of the center-of-mass, however. The GFMC result has a slight dip in the central region which

does not appear in the variational results. This dip appears in only a very small fraction of the total volume because of the r^2 phase space factor. Nevertheless, it does have some consequences when calculating the alpha particle charge form factor. In the impulse approximation, the charge form factor can be obtained as the fourier transform of the one-body charge distribution.

In reality, though, the effects of two-body charge and current operators can be important even at relatively low momentum transfer. The effects of these two-body terms must be included in order to obtain meaningful comparisons with experimental results. Riska[42] has developed a method for constructing models of the exchange currents which satisfy the continuity equation:

$$\nabla \cdot \vec{j}_{ex} + i\,[V_{ij}, \rho] = 0, \tag{52}$$

with an essentially arbitrary two nucleon interaction V_{ij}. Terms in the interaction can be identified which have the appropriate quantum numbers for pion or rho exchange. The continuity equation can then be used to constrain the pi- and rho-exchange terms in the current, which are called 'model-independent' because they are obtained directly from the interaction. In addition, there are transverse pieces in the current (e.g. $N\Delta\gamma, \rho\pi\gamma$, and $\omega\pi\gamma$) which are not so constrained. The most important two-body terms in the current are due to the pion:

$$j_\pi(q) = -3i(\tau_i \times \tau_j)_z[\tilde{v}_\pi(k_j)\vec{\sigma}_i(\sigma_j \cdot k_j) - \tilde{v}_\pi(k_i)\vec{\sigma}_j(\sigma_i \cdot k_i) -$$

$$\frac{\vec{k}_i - \vec{k}_j}{k_i^2 - k_j^2}(\sigma_i \cdot k_i \sigma_j \cdot k_j)[\tilde{v}_\pi(k_j) - \tilde{v}_\pi(k_i)]]G_E^V(q), \tag{53}$$

where k_i is the momentum transferred to nucleon i and $\tilde{v}_\pi$ is the fourier transform of the terms in the interaction associated with the quantum numbers of exchanged pions. In the limit of point pions and nucleons,

$$\tilde{v}_\pi(k) \rightarrow \frac{1}{3}\frac{f_\pi^2}{m_\pi^2}\frac{1}{k^2 + m_\pi^2} \tag{54}$$

Riska's method determines $\tilde{v}_\pi(k)$ and $\tilde{v}_\rho(k)$ directly from the interaction. In fact, this method produces nearly point-like pi- and rho-propagators with the Argonne interaction.
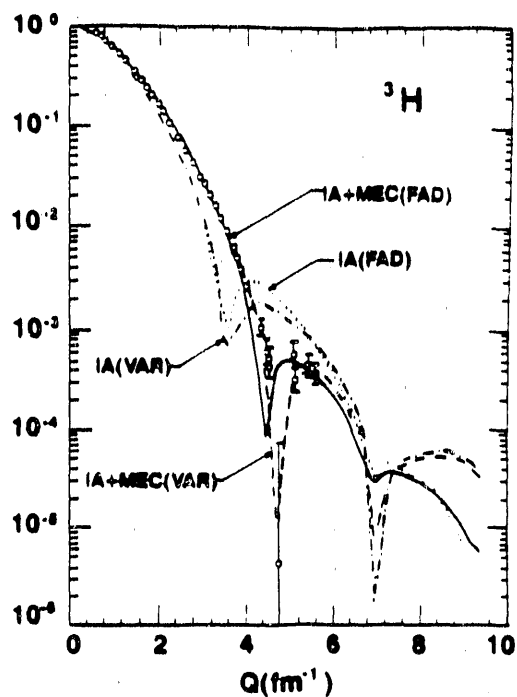
Figure 8a) Magnetic form factor of ^{3}H, from Schiavilla and Riska.[43] Impulse approximation (IA) results are shown along with the complete results (IA+MEC). Curves labeled FAD employ the exact Faddeev wave function, and variational results are labeled VAR.
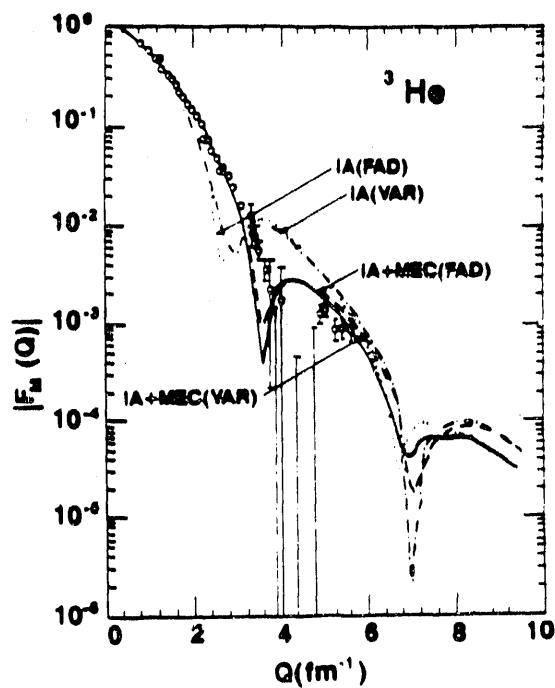

Figure 8b) Magnetic form factor of ^{3}He, as above.

Schiavilla and Riska have computed the magnetic form factors of ^{3}He and ^{3}H (Fig. 8) with this method, as well as the backward cross-section for the electrodisintegration of the deuteron. Several sets of curves are included in the figure, including results with the impulse currents alone and impulse plus two-body currents. In addition, the form factors obtained with Variational Monte Carlo and Faddeev methods are compared. The two sets of calculations give very similar results, although there are some differences in the region of the diffraction minimum and beyond. Clearly, the contributions of the exchange currents are crucial to reproducing the experimental results, particularly the contribution of the isovector exchange current operators. Schiavilla and Riska have also calculated the backward electrodisintegration of the deuteron near threshold. This reaction is also very sensitive to the isovector exchange currents, and is well reproduced in the calculations up to very high values of the momentum transfer.

They have also computed the charge form factors of the three-body nuclei[44] and obtain good agreement with experimental results. Exchange corrections to the charge operator are more speculative since they contain relativistic corrections[45] and are not constrained by the continuity equation. Some of these ambiguities are eliminated in the alpha particle however due to the fact that the alpha particle is an isoscalar system. We have combined the following one-body charge operator:

$$
\begin{aligned}
\rho_1(q) = & [1 - \frac{q^2}{8m^2}]\frac{1}{2}[G_E^S(q) + G_E^V(q)\tau_z] \\
& - \imath \frac{\sigma \cdot q \times P}{8m^2}\frac{1}{2}\left\{ [G_E^S(q) - 2G_M^S(q)] + [G_E^V(q) - 2G_M^V(q)]\tau_z \right\}.
\end{aligned}
\tag{55}
$$

incorporating the Darwin-Foldy term and a small $L \cdot S$ correction, with a two-body charge operator due to pions:

$$
\begin{aligned}
\rho_\pi(q) = \frac{3}{2m}\{ & \left[F_1^S(q)\tau_i \cdot \tau_j + F_1^V(q)\tau_{jz}\right](\sigma_i \cdot q\sigma_j \cdot k_j)\tilde{v}_\pi(k_j) + \\
& \left[F_1^S(q)\tau_i \cdot \tau_j + F_1^V(q)\tau_{iz}\right](\sigma_j \cdot q\sigma_i \cdot k_i)\tilde{v}_\pi(k_i) \}
\end{aligned}
\tag{56}
$$

to calculate the charge form factor of the alpha particle. This form of charge operator was first considered by Kloet and Tjon in examining pion photoproduction.[46] We have also included the remaining terms of Schiavilla and Riska, but their effect is an order of magnitude smaller than the terms above up to a momentum transfer of ≈ 5.5 fm^{-1}.

The contributions of the one-body and pion-exchange terms are shown in Fig. 9. The Variational and GFMC results for the pion-exchange term are nearly identical. There are some differences, though, in the calculated one body terms in the region of the second maximum. The form factor here is down by two orders of magnitude here, as there is a delicate cancellation in the fourier transform of the one-body density. Consequently, even a small difference in the density can make significant changes in the charge form factor.
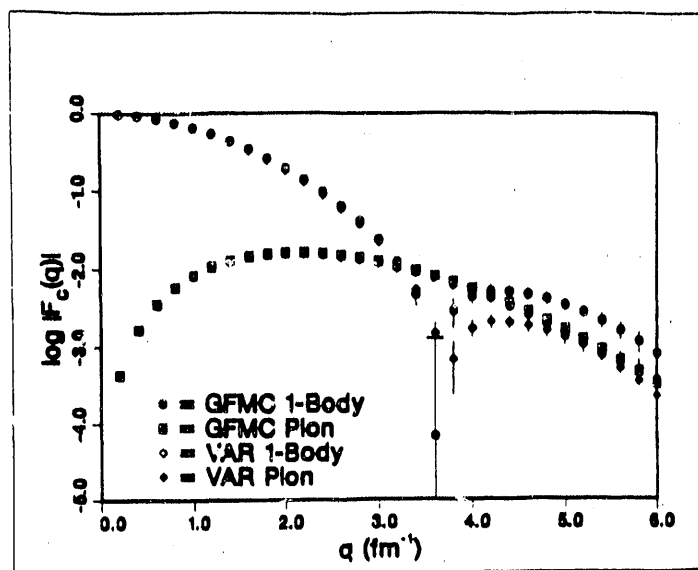
31

Figure 9) VMC and GFMC results for one-body and pion contributions to the alpha particle charge form factor.

The full calculations are compared to experimental results in Fig. 10. The GFMC calculation is in excellent agreement with experimental results up to a momentum transfer of ≈ 4.5 fm^{-1}. Beyond that point, the calculated form factor is significantly larger than experimental results. Nevertheless, the overall agreement is excellent, particularly at lower momentum transfers where one would expect the theory to work best.
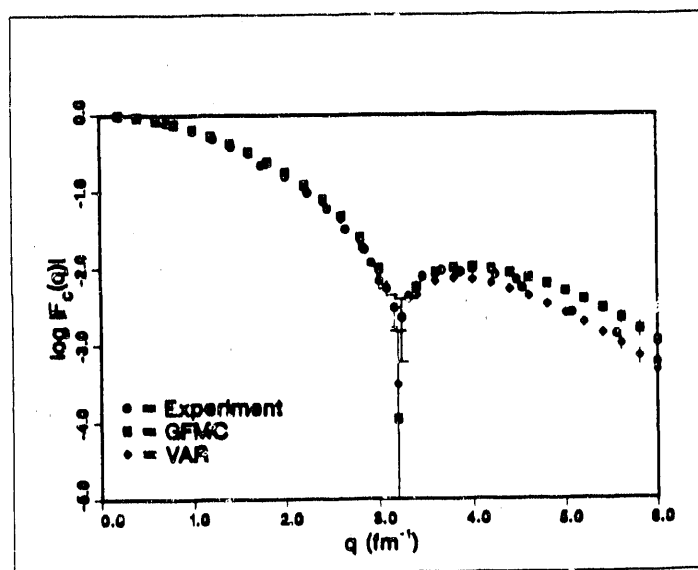

Figure 10) Alpha particle charge form factor, experimental and calculated.

Another very important goal in nuclear physics has been to obtain an experimental determination of the correlations of nucleons within a nucleus. Inclusive electron scattering experiments can measure the Coulomb sum, which provides a useful tool for studying these correlations. The Coulomb sum is defined as:

$$S = \frac{1}{Z} \int_{\omega_{el}^+}^{\infty} \frac{R_L(q,\omega)}{[G_E(q^2)]^2} d\omega, \tag{57}$$

where R_L is the longitudinal response of the nucleus and G_E is the proton form factor. The integral extends from energies just above elastic scattering to infinity, and hence we can use closure to calculate the Coulomb sum as a ground state expectation value.

$$S = \frac{1}{Z} \left[\langle 0| \sum_{j=1}^{A} \rho_j^\dagger(q) \sum_{k=1}^{A} \rho_k(q)|0\rangle - \frac{[Z F_c(q^2)]^2}{[G_E(q^2)]^2} \right], \tag{58}$$

where

$$\rho_k(q) = \exp(iq \cdot r_k)[\frac{1 + \tau_{zk}}{2}] \tag{59}$$

if we ignore small neutron contributions (which are included in the calculations) and two-body terms. In this approximation, the Coulomb sum is simply:

$$S = 1 - Z \frac{F_c(q^2)]^2}{[G_E(q^2)]^2} + \frac{1}{Z} \rho_{pp}(q), \tag{60}$$

where F_c is the charge form factor of the nucleus and $\rho_{pp}(q)$ is the fourier transform of the two-body distribution function integrated over the pair's center-of-mass.
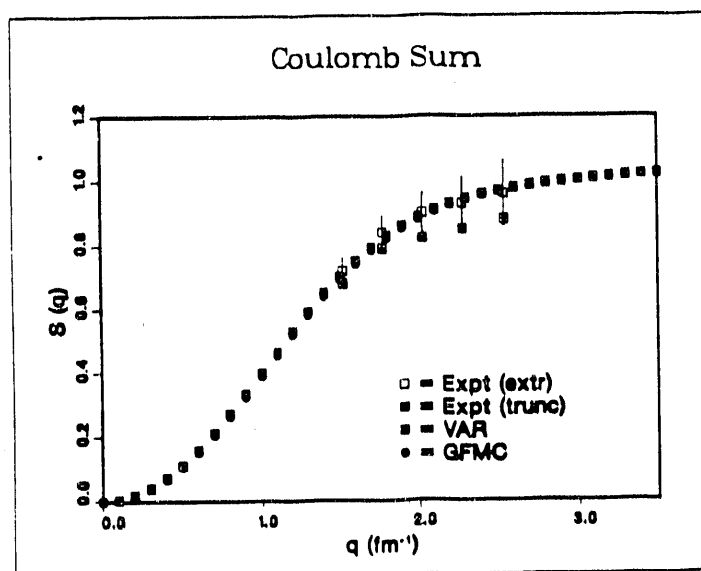

Figure 11) Coulomb sum in the alpha particle.

The calculations are compared to experimental results in Figure 11. Two caveats should be noted concerning this comparison. First, the experimental results only extend to a finite energy, and consequently must be extrapolated to determine the full Coulomb sum. Schiavilla et al.[47-49] calculated the energy- and energy-squared weighted sum rules with a variational wave function; assumed a functional form for the response in the tail region, and fit this curve to the calculated moments. The contributions of the tail region in the experiment are given by the difference between the points labeled 'extr' and 'trunc'. The latter includes only the response up to the experimental limit. As shown in the figure, the VMC and GFMC curves are nearly identical, and both agree very well with the extrapolated results.

Beck[50] has extracted $\rho_{pp}(q)$ from the experimental results in the three-nucleon system, and obtained the curve shown in Figure 12. He combined the experimental Coulomb sum and charge form factor, the results of Schiavilla, et al. for the (small) neutron contributions, and a slightly different extrapolation technique to produce the results shown in the figure. Although the qualitative features of the experimental and theoretical curves are similar, the experimental $\rho_{pp}(q)$ is much higher beyond the first minimum. This would indicate even a stronger correlation in the protons than is present theoretically, but contributions of two-body operators to the Coulomb sum should be included before strong conclusions are drawn.
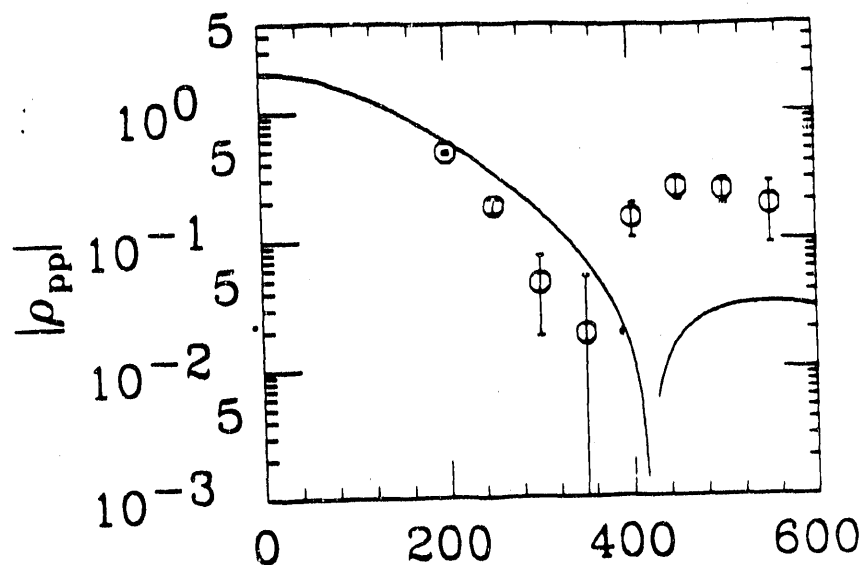

Figure 12) 'Experimental' vs. calculated (solid line) $\rho_{pp}(q)$, q in MeV, from Beck.[50]

Two important avenues are open for future research once a consistent picture of light nuclei has been obtained. The first of these is calculations of the structure and properties of heavier nuclei. The methods I have described in these lectures can be directly extended only up to approximately A=8, and work in this area is

currently under way. Beyond A=8, better methods have to be developed to handle the spin-isospin degrees of freedom in the nucleus. Important progress in this regard has been made by Pieper et al.,[51] who have employed a cluster summation technique to study ^{16}O. To date, variational calculations with the Argonne V14 plus TNI model 7 interaction (which is more attractive than model 8) give approximately 7 MeV binding per nucleon out of the experimental 8 MeV. They are currently working on improvements to both the variational wave function and the cluster summation methods. Improvements to the variational wave function incorporate two-body $L \cdot S$ correlations as well as improved three-nucleon correlations.

The other outstanding problem in the application of Monte Carlo methods to nuclear physics is the study of dynamic properties, a very ambitious goal. The primary successes to date have been in the study of low-energy scattering and electromagnetic transitions, as well as in approximate treatments of dynamic response in electron scattering.[52,53] I will concentrate on the former topic, and particularly upon the $n + {}^3He \rightarrow \alpha + \gamma$ reaction.

Variational Monte Carlo methods can be employed to study low-energy scattering in a regime where only two-body breakup is energetically allowed.[54] The basic idea is similar to R-matrix approaches, one studies eigenstates of the Hamiltonian in which there is no net flux in or out in any channel. In a one-channel problem this amounts to specifying a boundary condition at a radius beyond the interaction region and then performing a variational calculation to determine the energy eigenvalue associated with that boundary condition. The boundary condition can take the form of either requiring the relative wave function to be zero at a specific radius,[54] or more generally requiring a specific logarithmic derivative.[55] Determining the eigenvalue as a function of the boundary condition is then equivalent to determining the phase shift as a function of energy.

In principle GFMC methods can also be used to study these low-energy scattering problems, and consequently to systematically improve any variational results. This scheme can also be generalized to multi-channel scattering processes, but requires a determination of the energies and relative amplitudes at the channel surfaces. The method's practicality depends upon the ability to diagonalize in a small basis (10 - 20 states) using Monte Carlo methods. Preliminary results on small problems indicate that this should be feasible, but multi-channel methods have not been tested on a realistic problem.

We have used this method to study the $n + {}^3He \rightarrow \alpha + \gamma$ reaction.[55] At thermal energies this reaction is dominated the spin-1 s-wave scattering of neutrons on ^3He. Recent interest in this reaction has centered on its possible relationship to the weak capture process in the four-nucleon system, a reaction which produces the highest end-point energy neutrinos from the sun. There have been speculations that these neutrinos could be measured separately in a future solar neutrino observatory. In the impulse approximation, the weak and electromagnetic capture are closely related.

Our calculations indicate, though, that the radiative transition is dominated by exchange currents. We obtain a strong-interaction scattering length of 3.5 ± 0.25 fm for the spin one n-^{3}He state, which agrees well with experimental estimates. Using this scattering wave function and a variational ^{4}He wave function, we find that only 10 % of the experimental value (60 μbarns)[56] is obtained in the impulse approximation. The low value is to some extent understandable since the impulse cross section is precisely zero in the limit where there is no tensor force, and consequently a purely s-wave alpha particle.

Using the full exchange current models, we find a value of 110 μbarns for the cross section. Including only the 'model-independent' terms in the exchange currents gives 70 μbarns, in much better agreement with the experiment. A similar result is obtained if we keep only the π exchange terms, as has been done in the n-d capture calculations of Friar, Gibson, and Payne;[57] and use a cut-off of 5.8 π masses in the propagator. In this case we obtain a total cross section which agrees with the experimental value. Our results are quite sensitive to the scattering length, however, a decrease of 0.25 fm in the scattering length would increase the calculated cross sections considerably. We are currently investigating the application of these same methods to the weak capture of protons on ^{3}He. They have also recently been applied to the $d + d \rightarrow \alpha + \gamma$ reaction.[58]

7. Conclusion

Monte Carlo methods provide a valuable tool for understanding the structure and properties of quantum systems. I have concentrated on applications to light nuclei in these lectures, but these methods are equally applicable to other areas of nuclear physics, including hypernuclei and quark-model physics. In recent years we have developed a remarkably consistent picture of light nuclei with the help of Monte Carlo and Faddeev methods. Realistic nucleon-nucleon interactions combined with plausible three-nucleon-interaction models have been found to give a good description of the binding energy of three- and four-body nuclei. The calculations to date emphasize the important role of the tensor force, a primary component of this force being due to one-pion-exchange. When coupled with reasonable models of two-body exchange current and charge operators, these 'traditional' models also give remarkably good descriptions of three- and four-body electromagnetic form factors.

Light nuclei combine the advantages of relative computational simplicity (many realistic calculations are practical), with physical complexity. They offer an important laboratory for studying a wide variety of nuclear properties, including nucleon-nucleon correlations, weak and radiative transitions. These processes offer a wide variety of tests for the nuclear Hamiltonian and exchange current models. Heavier nuclei offer the opportunity for studying the nuclear interaction in negative parity states and very neutron-rich nuclei, which are important astrophysically through their connection with neutron stars.

The foremost challenge in the future lies in developing new methods to treat quantum dynamics and incorporating relativistic effects in few-body calculations. Some valuable progress has been made in both of these areas, but much remains to be done. Accurate microscopic calculations of the dynamic response of light nuclei to electromagnetic probes is perhaps the most important goal of the next decade.

References

1. J. Lomnitz Adler, V. R. Pandharipande, and R. A. Smith, Nucl. Phys. **A361**, 399 (1981).

2. J. Carlson, V. R. Pandharipande, and R. B. Wiringa, Nucl. Phys. **A401**, 59 (1983).

3. R. Schiavilla, V. R. Pandharipande, and R. B. Wiringa, Nucl. Phys. **A449**, 219 (1986).

4. J. Carlson and R. B. Wiringa, Los Alamos preprint LA-UR-90-411, to appear in *Computational Nuclear Physics*, Koonin and Langanke ed., Addison-Wesley.

5. M. H. Kalos, Phys. Rev. **128**, 1791 (1962).

6. M. H. Kalos, D. Levesque, and L. Verlet, Phys. Rev. **A9**, 2178 (1974).

7. K. E. Schmidt, in *Models and Methods in Few-Body Physics*, Lecture Notes in Physics 273 (Springer-Verlag, Berlin, 1987).

8. K. E. Schmidt, M. H. Kalos, and G. V. Chester, Phys. Rev. Lett. **47**, 807 (1981).

9. David A. Huse and Veit Elser, Phys. Rev. Lett. **60**, 2531 (1988).

10. M. H. Kalos, M. A. Lee, P. A. Whitlock and G. V. Chester, Phys. Rev. **B24**, 115 (1981).

11. R. M. Panoff and J. Carlson, Phys. Rev. Lett. **62**, 1130 (1989).

12. K. E. Schmidt and J. W. Moskowitz, J. Stat. Phys. **43**, 1027 (1986).

13. J. W. Moskowitz, K. E. Schmidt, M. A. Lee, and M. H. Kalos, J. Chem. Phys. **77**, 349 (1982).

14. K. Dow, et al., Phys. Rev. Lett **61**, 1706 (1988).

15. S. Dytman, et al., Phys. Rev. **C38**, 800 (1988).

16. K. F. von Reden, et al., Phys. Rev. **C41**, 1084 (1990).

17. R. B. Wiringa, R. A. Smith, and T. L. Ainsworth, Phys. Rev. **C29**, 1207 (1984).

18. R. Machleidt, K. Jolinde, and Ch. Elster, Phys. Rep. **149**, 1 (1987).

19. M. M. Nagles, T. A. Rijken, and J. J. de Swart, Phys. Rev. **D17**, 768 (1978).

20. C. R. Chen, G. L. Payne, J. L. Friar, and B. F. Gibson, Phys. Rev. **C33**, 1740 (1986).

21. J. L. Friar, in *New Vistas in Electro-Nuclear Physics* , ed. E. L. Tomusiak, H. S. Caplan and E. T. Dressler, Plenum, 1986.

22. B. F. Gibson and Bruce H. J. McKellar, Few-Body Systems **3**, 143 (1988).

23. Malvin H. Kalos and Paula A. Whitlock, *Monte Carlo Methods, Vol. I*, John Wiley and Sons, Inc., New York, 1986.

24. N. Metropolis, A. W. Rosenbluth, M. N. Rosenbluth, A. H. Teller, and E. Teller, J. Chem. Phys. **21**, 1087 (1953).

25. R. B. Wiringa, to be published.

26. J. Carlson, Phys. Rev. **C38**, 1879 (1988).

27. D. M. Ceperley and B. J. Alder, J. Chem. Phys. **81**, 5833 (1986).

28. D. M. Ceperley and E. L. Pollock, Phys. Rev. Lett. **56**, 351 (1986).

29. E. L. Pollock and D. M. Ceperley, Phys. Rev. **30**, 2555 (1984).

30. D. L. Scalapino and R. L. Sugar, Phys. Rev. Lett. **46**, 519 (1981), and R. Blankenbecler, D. J. Scalapino, and R. L. Sugar, Phys. Rev. **D24**, 2278 (1981), and Phys. Rev. **B24**, 4295 (1981).

31. M. A. Lee, K. E. Schmidt, M. H. Kalos, and G. V. Chester, Phys. Rev. Lett. **46**, 728 (1981).

32. D. M. Ceperley and B. J. Alder, Phys. Rev. Lett. **45**, 566 (1980).

33. R. M. Panoff, in *Condensed Matter Theories*, edited by R. Kalia, P. Vashishta, and R. Bishop (Plenum, New York, 1987), Vol. II.

34. R. A. Aziz, V. P. S. Nain, J. S. Cerley, W. L. Taylor, and G. T. McConville, J. Chem. Phys. **70**, 4330 (1979).

35. J. Carlson, Phys. Rev. **C36**, 2026 (1987).

36. J. Carlson, Nucl. Phys. **A508**, 141c (1990).

37. J. Carlson, to be published.

38. J. Carlson, presented at the Symposium in Honor of Akito Arima, Santa Fe, NM, 1990; Los Alamos preprint LA-UR-90-2258.

39. R. B. Wiringa, V. Fiks, and A. Fabrocini, Phys. Rev. **C38**, 1010 (1988).

40. B. F. Gibson, private communication.

41. Steven C. Pieper, private communication.

42. D. O. Riska, Physica Scripta, **31**, 471 (1985).

38

43. R. Schiavilla and D. O. Riska, Phys. Lett. **B244**, 373 (1990).

44. R. Schiavilla, V. R. Pandharipande, and D. O. Riska, Phys. Rev. **C41**, 309 (1990).

45. J. L. Friar, Phys. Rev. **C22**, 796 (1980), and in *Mesons in Nuclei*, M. Rho and D. H. Wilkinson, ed., North-Holland, 1979.

46. W. Kloet and J. Tjon, Phys. Lett. **49B**, 419 (1974).

47. R. Schiavilla, A. Fabrocini, and V. R. Pandharipande, Nucl. Phys. **A473**, 290 (1987).

48. R. Schiavilla, et al., Nucl. Phys. **A473**, 267 (1987).

49. R. Schiavilla, V. R. Pandharipande, and A. Fabrocini, Phys. Rev. **C40**, 1484 (1989).

50. D. H. Beck, Phys. Rev. Lett. **64**, 268 (1990), and U. of Ill. preprint (NPL)-90-006 (Panic XII invited talk, MIT, June 1990).

51. Steven C. Pieper, R. B. Wiringa, and V. R. Pandharipande, Phys. Rev. Lett. **64**, 364 (1990).

52. R. Schiavilla and V. R. Pandharipande, Phys. Rev. **C36**, 2221 (1987).

53. R. Schiavilla, Phys. Lett. **B 218**, 1 (1989).

54. J. Carlson, V. R. Pandharipande, and R. B. Wiringa, Nucl. Phys. **A424**, 47 (1984).

55. J. Carlson, D. O. Riska, R. Schiavilla, and R. B. Wiringa, Phys. Rev. **C 42**, 830 (1990).

56. F. L. H. Wolfs, S. J. Freedman, J. E. Nelson, M. S. Dewey, and G. L. Greene, Phys. Rev. Lett. **63**, 2721 (1989).

57. J. L. Friar, B. F. Gibson, and G. L. Payne, to appear in Phys. Lett. **B**.

58. A. Arriaga, R. Schiavilla, and V. R. Pandharipande, U. of Ill. preprint.

Appendix

Monte Carlo calculations of light nuclei are performed in a basis of definite third components of spin and isospin for each particle. Thus, the wave function at a given point in space can represented as a set of $2^A A!/(N!Z!)$ complex coefficients. The simplest case is the deuteron, where:

$$\Psi_d = f^c(r_{12})[1 + u^S(r_{12})S_{12}]\Phi_d, \tag{61}$$

and

$$\Phi_d = (n \uparrow p \uparrow -p \uparrow n \uparrow). \tag{62}$$

The uncorrelated state Φ_d, then, has only two non-zero coefficients and does not depend upon the spatial coordinates of the particles.

This basis of states is convenient because the spin-isospin operators take a particularly simple form. For example,

$$\sigma_i \cdot \sigma_j = 2P_{ij}^\sigma - 1, \tau_i \cdot \tau_j = 2P_{ij}^\tau - 1,$$

where $P_{ij}^{\sigma(\tau)}$ is a permutation operator in spin (isospin) space. Therefore, the $\sigma_i \cdot \sigma_j$ and $\tau_i \cdot \tau_j$ operators acting on a state can be evaluated by only two multiplications of a scalar times the wave function rather than by full matrix multiplications. The permutation operators above can easily be represented as bit manipulations on the array indices within the computer. For example, the indices corresponding to the spin states of the deuteron can be taken as

$$
\begin{aligned}
\downarrow_2\downarrow_1 &\leftrightarrow & 0 \ \ 0 = 0 \\
\downarrow_2\uparrow_1 &\leftrightarrow & 0 \ \ 1 = 1 \\
\uparrow_2\downarrow_1 &\leftrightarrow & 1 \ \ 0 = 2 \\
\uparrow_2\uparrow_1 &\leftrightarrow & 1 \ \ 1 = 3,
\end{aligned} \tag{63}
$$

where the middle column is simply the binary representation of the spin state. Clearly, P_{ij}^σ acting on state 01 (1) gives 10 (2), etc.

In a similar manner, the tensor operator $S_{ij} = 3\sigma_i \cdot \hat{r}\sigma_j \cdot \hat{r} - \sigma_i \cdot \sigma_j$ can be rewritten using:

$$\sigma \cdot \hat{r} = \sigma_+\hat{r}_- + \sigma_-\hat{r}_+ + \sigma\hat{r}_0, \tag{64}$$

where

$$
\begin{aligned}
\sigma_+ &= (\sigma_x + i\sigma_y)/2 \\
\sigma_- &= (\sigma_x - i\sigma_y)/2 \\
\sigma_0 &= \sigma_z \\
\hat{r}_+ &= (x + iy)/r \\
\hat{r}_- &= (x - iy)/r \\
\hat{r}_0 &= (z)/r.
\end{aligned} \tag{65}
$$

The operators σ_+ and σ_- do nothing but raise and lower spins, respectively. Note that they differ from the usual raising and lowering operators by a normalization; these operators give unit coefficient when they flip a spin. Just as the $\sigma_i \cdot \sigma_j$ and $\tau_i \cdot \tau_j$ can be represented through permutation operators, the tensor operator can be represented as combinations of permutation and spin flip operators.

In this basis, we can explicitly construct the deuteron wave function. It is given by:

$$
\begin{aligned}
\Psi_d \;=\; & f^c(r)[1 + u^S(r)(3\hat{r}_0^2 - 1)][n\uparrow p\uparrow - p\uparrow n\uparrow] \\
& + f^c(r)[u^S(r)(3\hat{r}_0\hat{r}_+ - 1)][n\uparrow p\downarrow + n\downarrow p\uparrow - p\uparrow n\downarrow - p\downarrow n\uparrow] \\
& + f^c(r)[u^S(r)(3\hat{r}_+^2 - 1)][n\downarrow p\downarrow - p\downarrow n\downarrow].
\end{aligned}
\tag{66}
$$

Wave functions for larger nuclei are easily constructed through successive operations of pair correlation operators. The effect of the potential terms acting on the wave function can be calculated similarly.

-END-

DATE FILMED

11 / 29 / 90